Korean J. Chem. Eng., 39(7), 1902-1918 (2022)
DOI: 10.1007/s11814-021-1036-5

pISSN: 0256-1115
eISSN: 1975-7220

Performance of TFN nanofiltration membranes through embedding internally modified titanate nanotubes

Zeynab Fallahnejad*, Gholamreza Bakeri*,,†, and Ahmad Fauzi Ismail*****

*Chemical Engineering Faculty, Babol Noshirvani University of Technology, Babol, Iran
**Advanced Membrane Research Lab, Babol Noshirvani University of Technology, Babol, Iran
***Advanced Membrane Technology Research Centre (AMTEC), Universiti Teknologi Malaysia, 81310 Skudai, Johor Darul Takzim, Malaysia
(*Received 29 August 2021 • Revised 28 November 2021 • Accepted 2 December 2021*)

Abstract−High toxicity of water resources by heavy metal ions is common and membrane filtration is one the solutions to this problem. Titanate nanotubes (TNT) are generally used due to their unique characteristics such as mesoporous structure, and high specific surface area. In this study, the internal surface of TNT was coated through a novel in-situ polymerization method with various polymers to alter the property and size of inner surface of the nanotubes, and then was embedded in the polyamide layer of the nanofiltration membrane. The modified nanotubes were supposed to act as the channels for water transport and reject the multivalent/monovalent ions; this phenomenon was more pronounced in the modified nanotubes because of the reduction in inner diameter. Fourier transform infrared spectroscopy, X-ray diffraction and Brunauer-Emmett-Teller analysis were used to characterize the unmodified/modified nanotubes. Furthermore, the membranes were synthesized by in-situ interfacial polymerization of trimesoyl chloride and m-phenylenediamine containing 0.05 wt% nanotubes; the performance of the fabricated membranes in terms of pure water flux (PWF), contact angle, feed flux and Na^+ and Cu^{2+} rejections was studied. Generally, incorporation of the modified nanotubes improved the trade-off between the permeation and rejection. Among the fabricated membranes, the maximum PWF was 26.13 L m^{-2} h^{-1} for the membrane containing 0.05 wt% polystyrene modified TNT, 71.23% more than neat thin film membrane and without any significant change in the rejection; that can be related to the hydrophilicity of the nanotube and the formation of small cavities on the membrane surface.

Keywords: Titanate Nanotubes, Nanofiltration Membranes, Ion Separation, Water Transport, Cu^{2+}/Na^+ Ions

INTRODUCTION

Water is one of the most important materials in the world. About 71% of the world's total water supply is protected by saltwater and the people are living with the remaining 29% and need fresh water to continue their life [1]. Global water supplies are inadequate to meet the population's water demands, which are rapidly increasing [2]. Conventionally, a number of technologies such as coagulation, adsorption, chemical precipitation, ion exchange, coagulation, flocculation, flotation, electrochemical and membrane filtration have been used for water purification. The advantages of membrane technology compared to the conventional ones are more productivity and modularity, ease in application and environmental friendliness [3,4]. In addition, the membrane with high water permeability and selectivity reduces the energy consumption [5].

Due to the lower energy consumption, membrane based water treatment processes have become the dominant purification techniques [6-8]. Nanofiltration (NF) can be used as a pretreatment method for the reverse osmosis (RO) seawater desalination process, which eliminates efficiently most of the divalent/multi-valent ions (Mg^{2+}, Ca^{2+}, SO_4^{2-}, etc.) from seawater as nicely as some of the monovalent ions (Na^+, K^+, Cl^-, etc.), therefore reducing the operating loads on the RO systems [9,10].

NF membranes are characterized by the pore size in the range of 0.5-2 nm, according to the MWCO of 200 to 2,000 Da. The lack of tuning on the membrane pores greatly limits the development and ability of NF process in membrane-based separations, especially for molecular-level ion/organic solute [11,12]. Compared to reverse osmosis, NF offers greater separation capability, specific performance and lower operating pressure [13]. Because of higher salt rejection than ultrafiltration (UF) membranes and lower energy consumption than RO membranes, nanofiltration membranes have been widely used in the water treatment sectors, including removal of the organic pollutants from surface water, wastewater purification and brackish water desalination [14,15].

NF can eliminate effectively many of the contaminants, such as ionic compounds, from the reclaimed water [16]. Mercury, copper, arsenic, nickel, cadmium and lead are the most common heavy metal ions that are found in the contaminated industrial wastewaters [17]. High toxicity by the heavy metal ions is commonly found in the water resources which are polluted by the industrial waste from the coal, textile and paint industries [18]. Cu(II) plays an important role in the human biochemistry, but just very small amounts of Cu(II) are required [19].

The membranes that are used in the NF process are generally thin film composite (TFC) membranes which are produced through

†To whom correspondence should be addressed.
E-mail: bakeri@nit.ac.ir
Copyright by The Korean Institute of Chemical Engineers.

the interfacial polymerization (IP) method where the active polyamide (PA) layer is formed through the reaction between the monomers that are dissolved in two organic and aqueous solvents [20,21]. Furthermore, in the thin film nanocomposite membrane (TFN), nanomaterials are incorporated in the polyamide layer which is an effective strategy to overcome the permeability-selectivity trade-off [22,23]. Commercial NF membranes are primarily thin film composite, consisting of polyamide selective layer and a porous sublayer membrane. However, many researches have been carried out to find novel approaches or materials for the preparation of selective layer of NF with superior permeability, selectivity, fouling resistance and stability [24,25]. The performance of the polyamide thin film membrane depends strongly on its morphology, structure and thickness. A typical dense polyamide layer is formed using trimesoyl chloride (TMC) as the organic phase monomer and m-phenylenediamine (MPD) as the aqueous phase monomer, which makes a selective layer with low permeability [26]. In addition, the surface of the polyamide layer is traditionally rough; that is linked to the diffusion of amine monomers (e.g. m-phenylenediamine (MPD)) into the organic acylchloride solution (e.g. trimesoyl chloride (TMC)) and the less stable reaction interface [27]. Furthermore, because of the large number of unreacted carboxylic acid groups in the PA layer, the membrane surface is negatively charged, which enhances the Donnan repulsion to reject the multivalent ions such as SO_4^{2-}, CO_3^{2-} and PO_4^{3-} [28].

Different approaches have been suggested to enhance the permeability of the polyamide based NF membranes, which the incorporation of nanomaterials is the most common method and can enhance the free volume and hydrophilicity of the selective PA layer [29,30]. Many studies reported the enhancement in the water permeability of the TFN membranes, using the nanomaterials without any internal pores/channels, which can improve the hydrophilicity of the membrane [31]; therefore, the nanomaterials should be hydrophilic and readily available with nontoxic characters to minimize the manufacturing costs and environmental impacts [32].

TiO_2 is one of the inorganic materials of particular concern that can be used in inorganic and organic nanocomposites [33], and due to its favorable atomic structure, TiO_2 possesses remarkable chemical and physical properties [34]. In addition, titanate nanotubes (TNTs) show excellent ion-exchange characteristics, particular properties due to its mesoporous features [35], highly ordered array structure, good mechanical and chemical stability and large specific surface area [36].

Rajaeian et al. [37] used aminosilanized TiO_2 nanoparticles to improve the salt rejection to 54% and water flux of NF membranes to 12.3 L m^{-2} h^{-1} at low concentration of NPs (0.005 wt%). Emadzadeh et al. [38] used amine functionalized TNTs (NH_2-TNTs) to avoid TNT agglomeration in the PA layer of TFN, and the modified membrane containing 0.05 wt% NH_2-TNTs showed water flux two-times greater without any reduction in the salt rejection. Kedchaikulrat et al. [39] synthesized TiO_2 NPs by sol-gel method and applied them in the MPD solution; the results showed that the water permeability and NaCl rejection improved up to 12% and 19%, respectively. Kumar et al. [40] synthesized phosphonic acid derivative of TiO_2 NPs and incorporated them in the PA layer of NF membrane, which improved the NaCl rejection up to 63%.

Modified TNTs were further used in ultrafiltration membranes. Szymanski et al. [41] modified titanate nanotubes with copper through the physicochemical process and incorporated them into the polyethersulfone UF membrane, which improved the water permeability and antifouling performance. Liu et al. [42] synthesized Ag doped GO/TNTs through dispersion of Ag NPs on the surface of GO/TNT and applied them in the composite membrane, which improved the water flux and dye rejection. Giel et al. [43] modified titanate nanotubes and used them in the gas separation membrane, which enhanced the selectivity. Delavar et al. [44] synthesized titanate nanotubes and blended them in the polyvinyl chloride mixed matrix UF membrane and increased the mean pore size and water flux. Azelee et al. [45] improved the surface properties of the membrane in terms of surface charge, surface roughness and contact angle through blending acid treated MWCNT-TNT (which was prepared by the hydrothermal method) in the PA layer and improved the water flux to 11.1 L m^{-2} h^{-1} at concentration of 0.05 wt% of NPs, while the rejection of NaCl/Na_2SO_4 was similar to the neat membrane. Hilder et al. [46] performed molecular dynamic simulation and reported that silicon nitride membrane with embedded boron nitride nanotubes can transfer water molecules and reject the ions to reach 100% salt rejection at high concentration of feed. Wei et al. [47] made water transport channels on the membrane surface through application of g-C_3N_4 NT/rGO composite and the membrane seems to be suitable candidate for the water purification, as well as provides a unique approach to develop membrane with enhanced photocatalytic characters. Das et al. [48,49] reported that CNT in NF/RO membranes can provide suitable routes for polar water molecules which reject ions and pollutants.

The objective of this research is the improvement of nanofiltration membranes using modified titanate nanotubes in the PA layer where the nanotubes are supposed to act as the channels for water transport and reject ions. At first, titanate nanotubes were synthesized and the inner surface of the nanotubes was coated with different polymers through a novel in-situ polymerization process to reduce the inner diameter of the nanotubes and control the passage of ions. Then, TFN membranes were synthesized and the water permeability and rejection of monovalent (Na^+) and divalent ions (Cu^{2+}) were investigated.

EXPERIMENTAL

1. Materials

Polysulfone was used as the base polymer for the preparation of the substrate for TFN membrane which was dried at 60 °C before using for the preparation of the casting solutions. N-methyl-2-pyrrolidone (NMP, purity: 99 wt%, BASF Co.), polyvinylpyrrolidone (PVP, purity: 99 wt%, Sigma-Aldrich) and Triton x-100 (purity: 99 wt%, Merck Co.) were used as the solvent, pore former and the surfactant for the fabrication of the substrate, respectively. Thin film composite membrane is made by the interfacial polymerization of m-phenylenediamine (MPD, purity: 99 wt%, Merck Co.) and Trimesoyl chloride (TMC, purity: 99.5 wt%, Merck Co.) on the polysulfone substrate. Hence, aqueous solution of MPD, which contains camphorsulfonic acid (CSA, purity: 99 wt%, Merck Co.) and tri-

ethyleneamine (TEA, purity: 99.5 wt%, Merck Co.) and TMC solution in n-hexane (purity: 96 wt%, Iran.) were applied for the preparation of polyamide selective layer. Commercial grade TiO_2 powder from Degussa (P25) was used for the preparation of titanate nanotubes through hydrothermal method. Analytical grade sodium chloride (NaCl, purity: 95 wt%) and copper sulfate pentahydrate ($CuSO_4 \cdot 5H_2O$, purity: 99 wt%, Merck Co.) were used for the rejection test of the TFN membranes.

To coat the internal surface of TNT12 by polyaniline, ammonium peroxodisulfate solution (APS, purity: 99 wt%, Merck Co.) as the initiator, aniline (purity: 99 wt%, Merck Co.) as the precursor and H_2SO_4 (purity: 95-98 wt%, Merck Co.) were used. Aniline was purified through distillation process to remove impurities before application. In addition, to coat the internal surface of TNT12 by polydopamine, dopamine hydrochloride (40 mg/mL, Caspian Tamin Pharmaceutical Co., Iran) was used as the monomer and NaOH (purity: 99 wt%, Iran) solution was used as the initiator for the polymerization process. Commercial grade styrene monomer (purity: 99 wt%, Baniar Polymer Gonbad, Iran), commercial grade methanol (as the solvent) and benzoyl peroxide (as the initiator, purity: 72-75 wt%, Merck Co.) were used for the internal coating of TNT12 by polystyrene. N1-(3-Trimethoxysilylpropyl) diethylenetriamine (purity: 99 wt%, Sigma Aldrich), a hydrophilic silane, was employed to improve the dispersibility of the nanoparticles in the MPD solution.

2. Synthesis of Titanate Nanotube (TNT)

Titanate nanotube was synthesized from TiO_2 nanoparticle by the hydrothermal method, which is commonly applied because of its flexibility [50]. The preparation of TNTs from TiO_2 nanoparticles through the hydrothermal process provides high surface area and large pores compared to other methods, in addition to the hydrophilic characteristic [51]. 5 gram commercial grade TiO_2 powder was dispersed in 250 mL of 10 M NaOH aqueous solution and subjected to hydrothermal treatment at 160 °C in a Teflon-lined autoclave for 12 h under autogenous static pressure. The precipitates were separated by filtration after cooling to room temperature and washed thoroughly with distilled water until

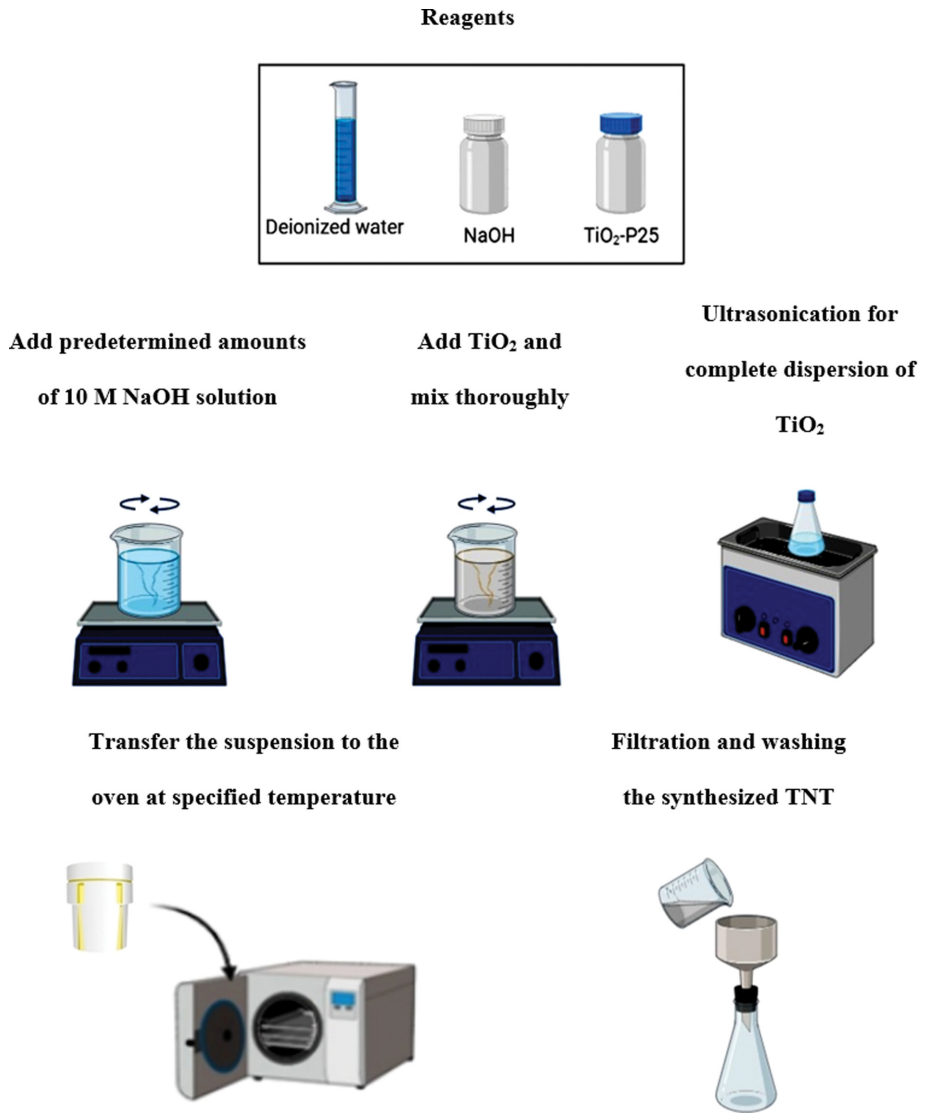


Fig. 1. The schematic of TNT synthesis process.

neutralization [52]. The schematic of TNT synthesis process is presented in Fig. 1. The prepared nanotube was named as TNT12.

3. Internal Coatings of Titanate Nanotubes (TNTs)

The general procedure for internal coating of TNTs involved dispersing the nanoparticles in the solvent through mixing and ultrasonication to make a homogeneous suspension. Then, the monomer was added and the mixture was delivered to a closed steel container and the pressure was reduced to 540 mmHg for 60 min to remove the air from the internal parts of the nanotubes; that makes the solution (which contains the monomer) to penetrate into the tubes. Then, the NPs were removed by filtration and washed thoroughly by the solvent to remove any monomer from the outer surface of NPs.

After that and in the second step, the NPs were dispersed again in the solvent and the initiator for the polymerization process was added; the pressure of the container was reduced to 540 mmHg for 60 min to make the initiator to be sucked to the tubes. Then, the mixture was mixed at specified temperature to complete the polymerization process. Finally, the modified NPs were separated by filtration, washed thoroughly by the solvent and dried at 60 °C for 12 h.

3-1. Polydopamine Coating of Titanate Nanotubes (PDTNT12)

In case of polydopamine coating, 5 mL dopamine hydrochloride solution (40 mg/mL) per gram of TNT was used as the monomer, 100 mL water was used as the solvent and 1 mL NaOH solution (2 M) was used as the initiator for the self-polymerization of dopamine. The pH of the solution was around 12. Furthermore, in the second step of the coating process, the NPs were mixed for 2 h at room temperature. A schematic of inner coating of TNT by polydopamine is depicted in Fig. 2. The polydopamine-coated TNT was named as PDTNT12.

3-2. Polyaniline Coating of Titanate Nanotubes (PATNT12)

Aniline is typically produced by the reduction of nitrobenzene and some impurities are present in the crude product; therefore, aniline was purified through total reflux distillation process at 100 °C for 60 min.

To coat the inner sides of TNTs with polyaniline, an aqueous solution of H_2SO_4 (2.8 mL H_2SO_4 98 wt% in 50 mL water) and aniline monomer (1 mL aniline per gram of nanotube) was used as the solvent and the precursor for the polymerization in the first step. In the second step, aqueous solution of ammonium peroxodisulfate (APS) (1 gram APS per gram of nanotube) was used as the initiator and the suspension was mixed at 0-3 °C for 3.5 h to complete the polymerization. A schematic of polyaniline polymerization process is depicted in Fig. S1. The polyaniline coated TNT was referred to as PATNT12.

3-3. Polystyrene Coating of Titanate Nanotubes (PSTNT12)

In the case of polystyrene coating and for 2 grams of nanotubes, styrene (4 grams) and methanol (70 mL) were used as the monomer and the solvent in the first step and in the second step; the solution of benzoyl peroxide (0.12 gram) in methanol (70 mL) was used as the initiator. Furthermore, in the second step of the coating process, the NPs were mixed for 3.5 h at room temperature. A schematic of polystyrene polymerization process is depicted in Fig. S2. The polystyrene coated TNT was named as PSTNT12.

4. Silanization of NPs

To improve the dispersibility of NPs in MPD solution during the synthesis of polyamide thin film, the NPs were modified by a hydrophilic silane. At first, NPs (1 gram) were added to water and mixed through ultrasonication for 1 h and then, N1-(3-Trimethoxysilylpropyl) diethylenetriamine (0.1 gram) was dissolved in the suspension and mixed for 1 h.

5. Characterization of NPs

X-ray diffraction (XRD), which is an important tool for evaluating the morphological characteristics of NPs [53], classifies the phase of a crystalline substance to determine the nature of the material as crystalline or amorphous. XRD analysis was done using Powder X-Ray Diffractometer, Bruker AXS-D8 Advance.

FTIR can provide qualitative analysis for organic and inorganic samples through producing an infrared adsorption spectrum; FTIR

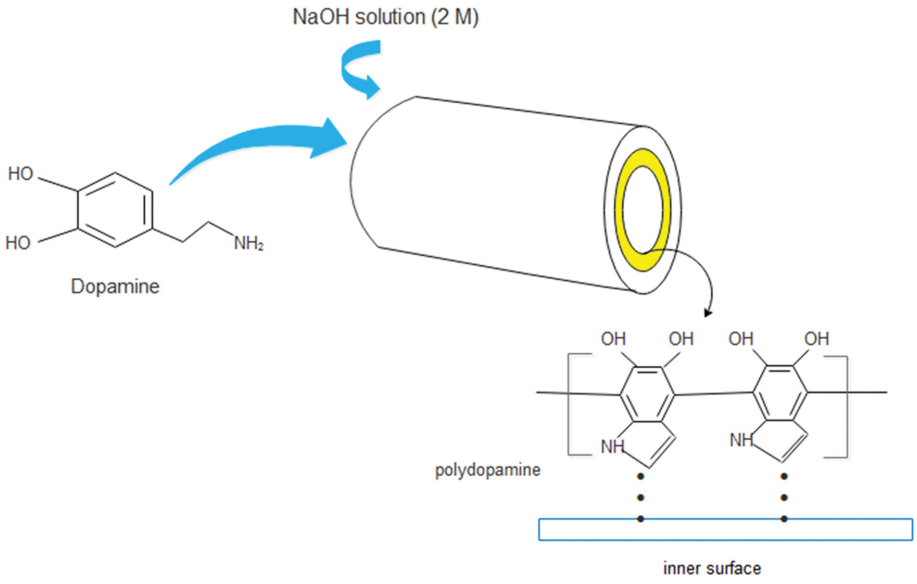


Fig. 2. The schematic of inner coating of TNT by polydopamine.

can recognize the chemical bonds inside the material. The FTIR test was done using Perkin Elmer-Spectrum 65. In addition, the TEM test was done to study the structure of the nanotubes before and after polydopamine and polystyrene coating using Philips, EM 208S.

The Brunauer-Emmett-Teller (BET) test uses the physical adsorption of gas molecules on the solid surface, which serves as the basis for the determination of the surface area and mean pore size of the materials [54]. In this study, BET test was done using BEL Japan Inc., Tokyo, Japan through N_2 adsorption/desorption measurements. Furthermore, the FESEM test was performed to study the shape and structure of the synthesized TNT NP. After coating with Au, the image was taken at 50 K magnification, using FESEM instrument, model: ZEISS Sigma.

The pH of point of zero charge (pH_{PZC}) for the synthesized nanoparticles was measured to determine the pH at which the charges on the surface of NPs are zero. At first, a number of 10 mL of 0.1 M NaCl solutions were prepared in different containers, and then the pH of the solutions was adjusted between and 2 and 10, using 0.1 M HCl and 0.1 M NaOH solutions. Then, 0.01 gram NPs was poured in the solutions and mixed for 48 h at room temperature and, finally, the pH of the solutions was measured. The pH_{PZC} was calculated through plot of ($pH_{final} - pH_{initial}$) versus $pH_{initial}$.

6. Preparation of PSf Substrate

PSf substrate was prepared via the phase inversion method. Predetermined amounts of PSf (14 wt%), triton x-100 (2 wt%) and PVP (1 wt%) were dissolved in NMP at 60 °C. The casting solution was then placed in the ultrasonic bath to remove the gas bubbles. Then, the polymer solution was cast on the clean glass sheet, using a glass rod and was immersed immediately in the deionized water (DI) bath. The fabricated PSf membranes were preserved in the water bath at room temperature for 24 h to remove any residual NMP solvent.

7. Preparation of Thin Film Nanocomposite (TFN) Membranes

The polyamide (PA) active layer was synthesized on the top surface of PSf substrate through interfacial polymerization (IP) process by the reaction of m-phenylenediamine (MPD) and trimesoyl chloride (TMC). In detail, predetermined amount of nanotubes (0.05 wt%) was dispersed through mixing and ultrasonication in aqueous solution containing 2 wt% MPD, 2 wt% comphorsulfonic acid and 1 wt% triethyleneamine. The PSf substrate was immersed in this suspension for 2 min; then it was removed and the excess aqueous solution on the surface of the membrane was collected using a soft rubber roller. Subsequently, the substrate was immersed in 0.1 wt% TMC/hexane solution for 10 seconds to initiate the interfacial polymerization process. Then, the TFN membrane was placed in the oven at 60 °C for 15 min to complete the reaction. Finally, the membrane was immersed in DI water. A schematic of TFN membrane preparation is depicted in Fig. S3.

8. Membrane Characterization

8-1. Porosity and Pore Size Measurement of the Substrate Membrane

To measure the porosity, some samples were immersed in methanol and then in water for a few days, respectively, to completely wet the membranes. Then, the weight of the wet membrane was measured by the balance. The samples were dried at 45 °C for 12 h and the weight of the dried membranes was measured. The porosity of the membrane was calculated using Eq. (1) [55]:

$$\varepsilon = \frac{\frac{\omega_1 - \omega_2}{\rho_\omega}}{\frac{\omega_1 - \omega_2}{\rho_\omega} + \frac{\omega_2}{\rho_p}} \quad (1)$$

where ω_1 is the weight of the wet membrane (gr), ω_2 is the weight of the dry membrane (gr), ρ_p is the density of the polymer (1.24 g cm^{-3} for PSf) and ρ_w is the density of the water (1 g cm^{-3}). The mean pore size (r_m) of the substrate membrane, which is a criterion for the pore size along the thickness, was measured by the pure water permeation test using Eq. (2) [55-59]:

$$r_m = \sqrt{\frac{8\eta l Q(2.9 - 1.75\varepsilon)}{\varepsilon A \Delta P}} \quad (2)$$

where η is the water viscosity (8.9×10^{-4} Pa s); l is the membrane thickness (m); ΔP is the transmembrane pressure difference (0.1 MPa); Q is the permeation flow rate ($m^3\ s^{-1}$) and A is the effective membrane area (m^2).

8-2. Nanofiltration Experiments

Fig. S4 shows the cross-flow nanofiltration setup where a stainless steel module with the effective membrane area of 32 cm^2 was used. The performance of the fabricated membranes in NF process, in terms of flux and rejection, was evaluated using NaCl (200 ppm NaCl) and $CuSO_4$ (500 ppm $CuSO_4$) aqueous solutions as the feed, while the experiments were performed at 5 bar pressure, room temperature and 240 min operating time.

Before each NF test, the membrane was compacted through pure water flux (PWF) test in which pure water flowed on the membrane and the pressure of water was increased to 7 bar and then, was decreased to 5 bar in a cyclic manner and during 1 h until the flux was stabilized. Then, the PWF of the membrane was calculated using Eq. (3).

$$J_w = \frac{V}{A \times \Delta t} \quad (3)$$

where J_w is the pure water flux, V (L) is the volume of the permeate, A (m^2) is the membrane area and Δt (h) is the sampling time. After compaction, the abovementioned feed solutions were used to measure the rejection and flux of the fabricated membranes. The concentration of ions in the permeate was measured using the conductivity meter (model: AZ 86505) and the rejection of the membrane was calculated through Eq. (4).

$$R = 1 - \frac{C_P}{C_F} \quad (4)$$

where R is the salt rejection, C_P and C_F are the ion concentrations in the permeate and feed solutions, respectively.

8-3. Scanning Electron Microscopy (SEM)

Scanning electron microscopy (SEM) is widely used in the material sciences, including polymeric membrane, to describe the microscopic structure due to its high lateral resolution and high focus depth. The membrane sample was broken in liquid nitrogen and then Au sputtering. and images were taken from the surface and cross section of the membrane.

8-4. Contact Angle Measurement

One important parameter that governs membrane wettability is the contact angle. The hydrophilicity of the membrane surface is evaluated through measuring the angle between a small drop of water and the membrane surface using the static contact angle method [60-62]. The water contact angle of the NF membrane was determined by the sessile drop method using the contact angle goniometer (Model: Sharif Solar, model: CA500). To minimize the error, the contact angle was measured at 15 points on the surface of the membrane and was averaged.

8-5. AFM Analysis

The surface roughness of the neat TFC membrane and TFN membrane containing 0.05 wt% TNT was studied using atomic force microscopy (AFM, Bruker Dimension Icon, USA). The root mean square (RMS) and root average arithmetic (R_a) were used to quantify the membrane surface roughness.

8-6. Attenuated Total Reflection-Fourier Transform Infrared Spectroscopy (ATR-FTIR) Analysis

ATR-FTIR spectroscopy was used to evaluate the functional groups of the TFC/TFN membranes. The analysis was performed with Perkin Elmer-Spectrum 65.

RESULTS AND DISCUSSION

1. Characterization of Modified/Unmodified Nanotubes

1-1. X-ray Powder Diffraction (XRD)

Fig. 3 displays the XRD spectra of the synthesized virgin titanate nanotube and the nanotubes internally coated with different polymers (polydopamine, polyaniline and polystyrene); there are no significant variations in the spectra that shows the coating of the internal parts of the nanotubes does not have any major influence on the structure of TNT, as was reported elsewhere [63]. The pure TNT reveals four main peaks at 2θ=10.21°, 24.82°, 39.242° and 48.76° which are the characteristics of the layered titanate monoclinic structure ($H_2Ti_3O_7$) [53]. In addition, there is little variation in the XRD patterns (Fig. 3) that can be linked to the amorphous

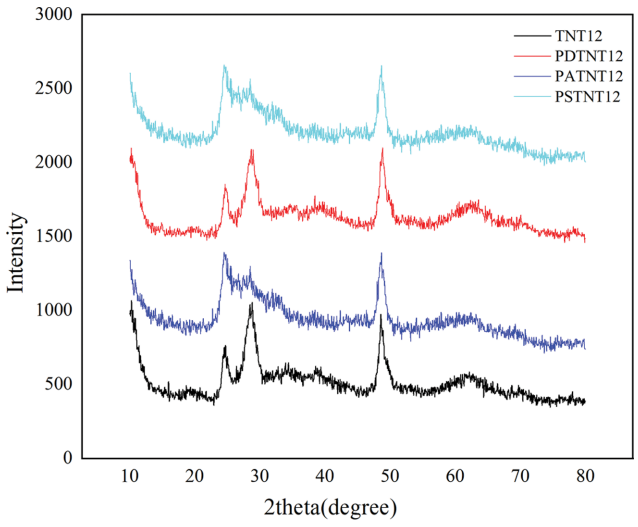


Fig. 3. XRD spectra of the synthesized TNT and internally coated TNT with different polymers.

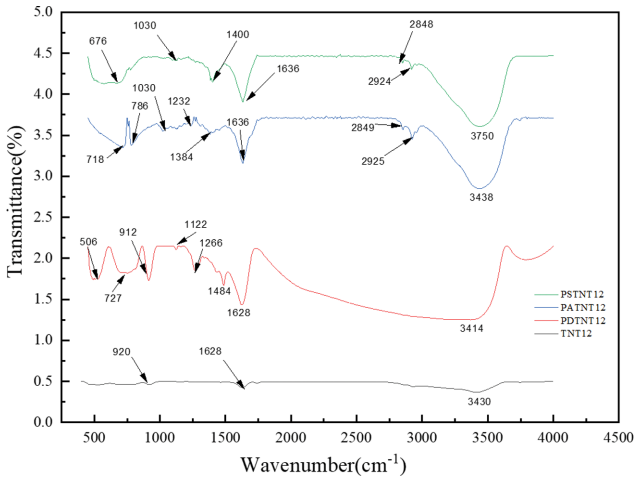


Fig. 4. The FTIR spectra of the synthesized TNT and internally coated TNT with different polymers.

structure of the coated polymers [63].

1-2. Fourier-transform Infrared Spectroscopy (FTIR)

Fig. 4 demonstrates the FTIR spectra of the synthesized titanate nanotubes coated with different polymers. The peaks at 920 cm^{-1}, 1,628 cm^{-1} and 3,300-3,450 cm^{-1} represent the vibration of Ti-O, H-O-H and surface OH groups of TNT, respectively [64]. Compared to the neat TNTs, PDTNT12 shows additional peaks between 1,000 cm^{-1} and 1,700 cm^{-1} that is linked to the polydopamine coating. The peaks at 912 cm^{-1}, 1,122 cm^{-1} and 1,266 cm^{-1} are assigned to C-O stretching, C-N and amide II bonds, respectively [65-67]. Additionally, the peaks at 1,628 cm^{-1} and 1,484 cm^{-1} are associated with the polydopamine indole unit (stretching of aromatic C-C bonds of indole) [67,68] and C-N bending in indole quinone unit [68,69], respectively. The wide peak in the 3,300-3,700 cm^{-1} range (3,414 cm^{-1}) can be assigned to the N-H and hydroxyl groups of polydopamine [68,70,71].

For PATNT12, the peak at 3,438 cm^{-1} is related to the N-H stretching of aromatic amines, and the peaks in the range of 2,849-2,925 cm^{-1} are linked to the aromatic C-H stretching. In addition, the bands at 1,384 cm^{-1} and 1,636 cm^{-1} are assigned to the C=N and C=C stretching benzenoid and quinoid ring vibrations in polyaniline [72-74]; that confirms successful coating. Furthermore, the peak at 1,232 cm^{-1} is assigned to the C-N stretching of benzenoid ring that is a feature of the conductive protonated form of polyaniline [75,76]. In addition, the peaks in the range of 1,000-1,200 cm^{-1} are related to the plane bending vibration of C-H bond, and the band at 786 cm^{-1} is related to the vibrational deformation of the aromatic C-H. Furthermore, the peak at 3,438 cm^{-1} is assigned to the O-H and N-H stretching vibrations [72,73]. The wide peak at 718 cm^{-1} is linked to the asymmetric Ti-O-Ti bond [77].

The FTIR spectra of PSTNT12 show aromatic C-H bond stretching vibration at 1,400 cm^{-1} and 1,637 cm^{-1}, deformation of the aromatic ring CH_2 and C=C at 1,030 cm^{-1} and 676 cm^{-1}, which confirms the existence of polystyrene coating [78].

1-3. Transmission Electron Microscope (TEM)

Fig. 5(a) shows the TEM image of the synthesized TNT which further demonstrates the tubular structure of TNT. The TEM images

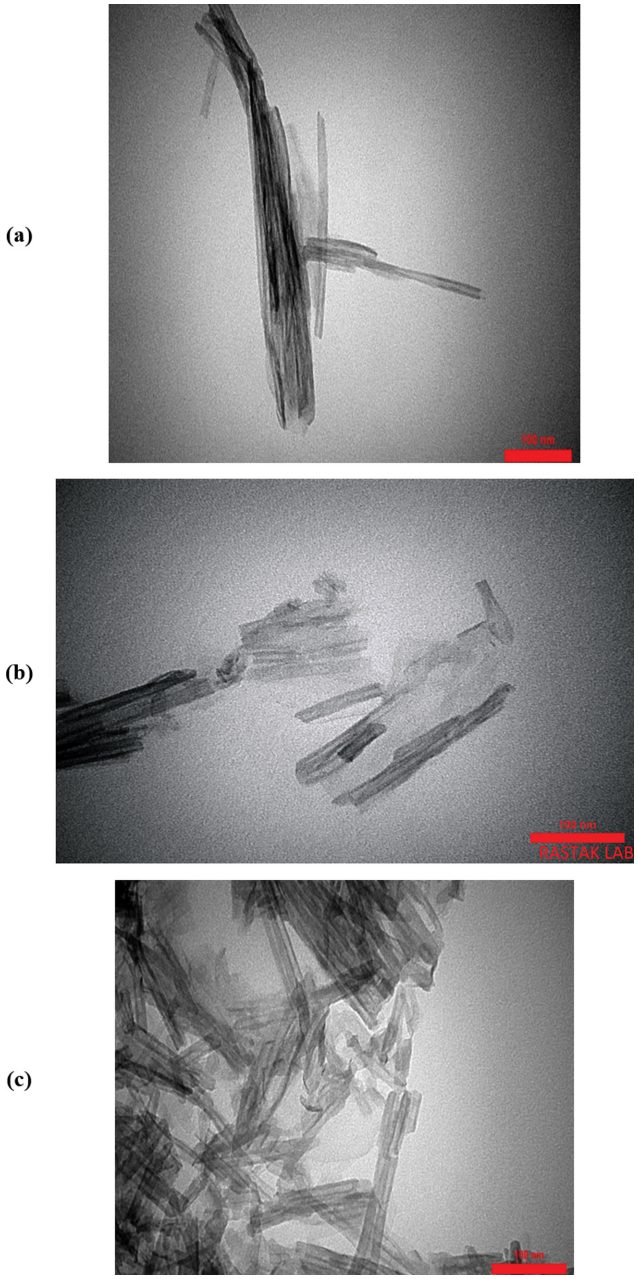


Fig. 5. TEM images of (a) TNT12, (b) PDTNT12 and (c) PSTNT12.

of the PDTNT12 and PSTNT12 are shown in Fig. 5(b) and Fig. 5(c), respectively, where the inner wall of the modified nanotubes seems to be slightly thicker than TNT12 with some light-gray lines on the inner surfaces; that can be related to the internal coating of the nanotubes. In addition, there is no deformation of TNT or coating of polymer on its outer surface.

Using the TEM images, the outer diameters of some nanotubes were measured (Fig. 6) and, then, the mean diameter was calculated; that is 11.1 nm, which is compatible with the results in other studies [79-81].

1-4. Brunauer-Emmett-Teller (BET) Test

The results of BET analysis for virgin and internally coated TNT are presented in Table 1 where v_m is the amount of the adsorbed

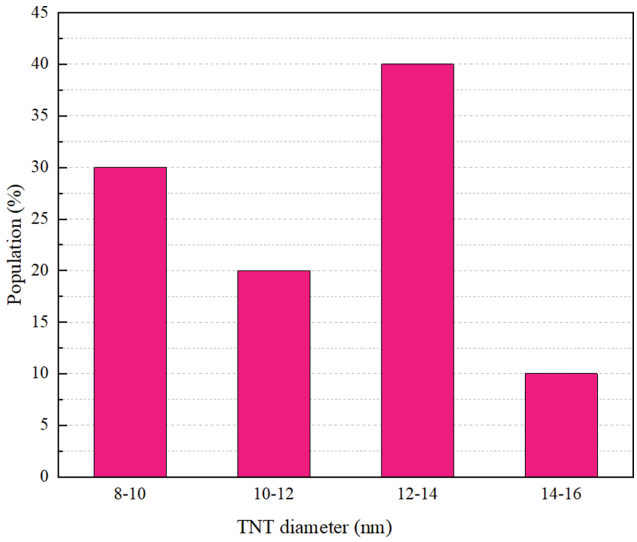
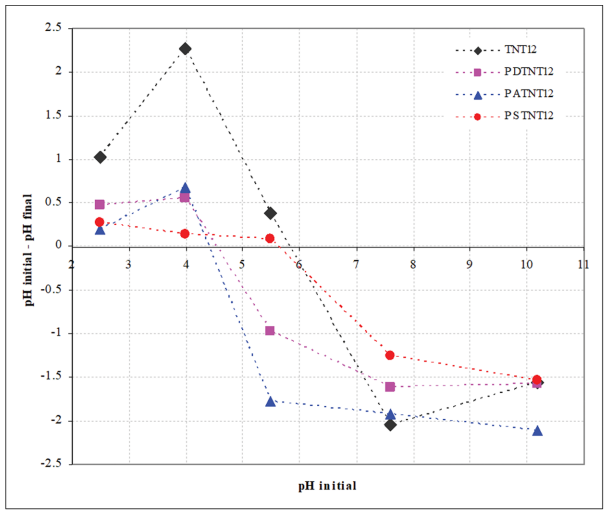


Fig. 6. The outer diameter histogram of the synthesized TNT.

Table 1. BET test results of TNT, PDTNT12, PATNT12 and PSTNT12

Nanotube	v_m ($cm^3\ g^{-1}$)	Specific surface ($m^2\ g^{-1}$)
TNT12	43.823	190.74
PDTNT12	17.996	78.326
PATNT12	53.775	234.05
PSTNT12	38.325	166.81



NP	TNT12	PDTNT12	PATNT12	PSTNT12
pH_{PZC}	5.77	4.50	4.40	5.63

Fig. 7. pH_{PZC} test results for the neat TNT, PDTNT, PATNT and PSTNT.

gas as a monolayer on the surface of the particle's inner cavities and can be a representative of the total volume of the pores. The results show that the volume of the pores decreased and that can be linked to the internal coating of TNT. In case of polyaniline coating, v_m increased, which may be related to the interaction of

the adsorbed gas with the polymer.

1-5. pH_{PZC} Test

The pH_{PZC} of the modified/unmodified nanotubes was measured and the results are shown in Fig. 7 where the pH_{PZC} of all NPs is less than 7; thus, at the experimental conditions for the salt rejection tests, the surface of the NPs is negatively charged, which makes repulsion to the anions of the salts (Donnan phenomenon) [82,83].

1-6. FESEM Test of the Unmodified Nanotube

Fig. S5 shows the FESEM of virgin TNT where the tubular structure of the synthesized particles is quite evident.

2. Membrane Characterization

The properties of the fabricated membranes were evaluated through different tests, such as porosity and pore size measurement, contact angle, permeation flux and rejection, where the results are presented as follows.

2-1. Characteristics of the Sublayer Membrane

The porosity and mean pore size of PSf sublayer membrane was measured using the procedures described in section 2.8.1; the membrane pore size and porosity are 15.7 nm and 87.8%, respectively.

2-2. Pure Water Flux of the Prepared NF Membranes

The nanotubes were blended into the MPD solution before polymerization and incorporated into the thin film composite membrane structure. Nanometer pathways are created through the nanotubes as well as the interface between the nanotube and the polymer matrix by inclusion the modified/unmodified nanotubes to the polyamide layer, causing an increase in the pure water flux. In TFN membrane, water can pass along the cross section of the membrane through both the body of the PA layer and the nanotubes. Even though the water permeation length through the nanotubes may be longer, the hydrophilic character of the nanotubes can promote the water penetration and enhance the water flux. Thus, the nanotubes can add extra channels to the polyamide layer and their tubular shape creates tiny pores that can improve the flux through the membrane. Thus, such paths can be considered as the distances with low resistances which allow water to penetrate faster; the nanotubes further enhance the hydrophilicity of the membrane.

A number of studies showed that blending the nanoparticles can improve the performance of the polyamide thin film membrane through creation of additional pathways for the passage of water [84-86]. The pure water flux of the neat TFC and TFN membranes containing 0.05 wt% TNT/modified TNT is presented in Fig. 8 where blending nanotubes enhanced the PWF of the NF membranes. Incorporation of the nanotubes in the polyamide layer of the NF membrane can create channels for water transport through the structure of the membrane [87] and further affect the hydrophilicity of the membrane, as TNTs contain hydrophilic groups (such as hydroxyl) on its surface which can bind with the water molecules [88,89]. In addition, the nanotubes can make some defects in the PA layer; these pathways with low resistance can allow water to penetrate faster and increase the permeation flux. On the other hand, the internal coating of TNT with the polymers can make interaction with the water molecules and facilitate the transfer of water through the nanotubes. It should further be considered that the arrangement of the nanotubes in the polyamide layer affects the distance that the water molecules should pass through the thickness of the membrane [90].

The water flux for TNT12 was greater than the neat TFC membrane, which is related to the channeling effect of TNT in the structure of the membrane and higher hydrophilicity, but the flux decreased for PDTNT12 and PATNT12; that can be connected to the reduction in the diameter of the nanotubes. In addition, the thickness of PA layer affects the permeation rate which, in case of TFN membranes, this can happen because of the interaction between MPD and TNT which lessens the concentration of MPD in the reaction zone. The reduction in PA thickness influences negatively the rejection as the defects can be created in the PA layer [91,92].

2-3. Feed Solution Permeation and Rejection of the Fabricated Membranes

The permeation flux of the feed solutions, 500 ppm $CuSO_4$ and 200 ppm NaCl, for the prepared membranes is presented in Figs. 9-10, respectively, where the flux is generally lower than the pure

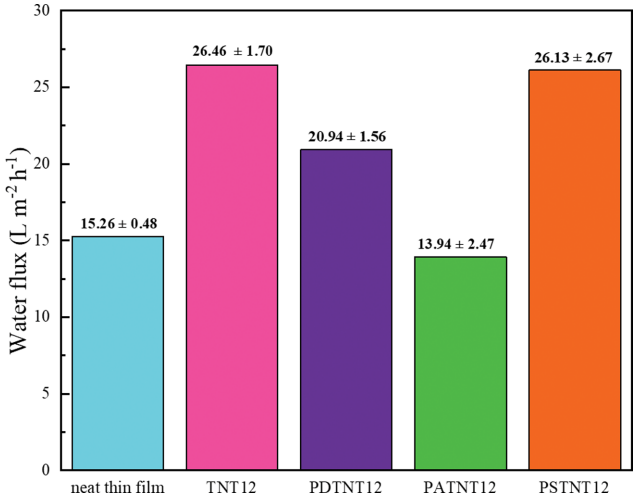


Fig. 8. The pure water flux of the neat membrane and the membranes modified with nanotubes at 5 bar.

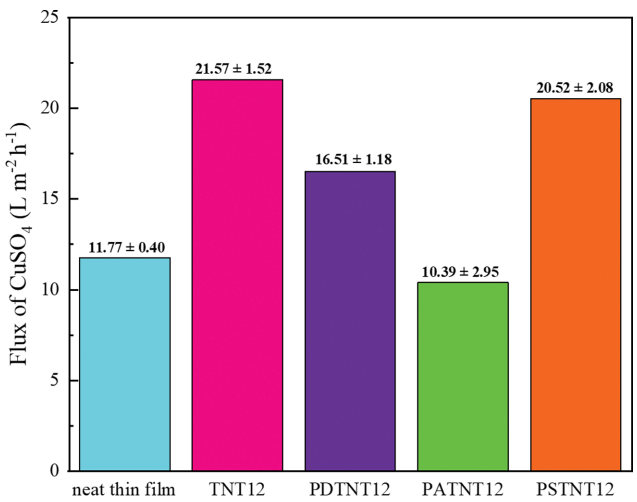


Fig. 9. Feed solution permeation flux (L/m^2 h) containing copper ion at constant pressure of 5 bar for the fabricated membranes.

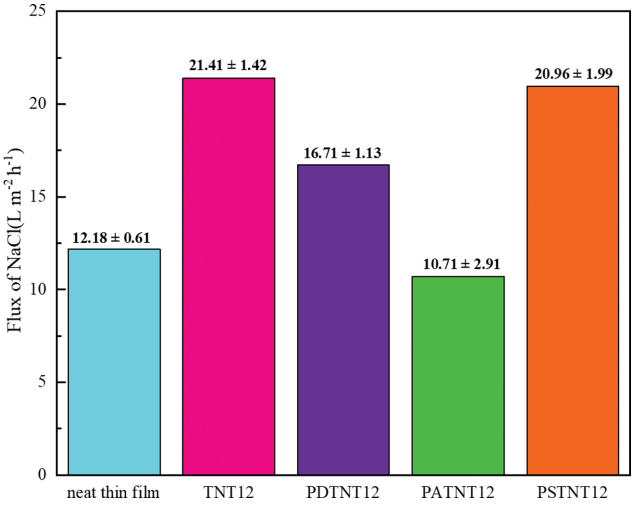


Fig. 10. Feed solution permeation flux (L/m^2 h) containing sodium ion at constant pressure of 5 bar for the fabricated membranes.

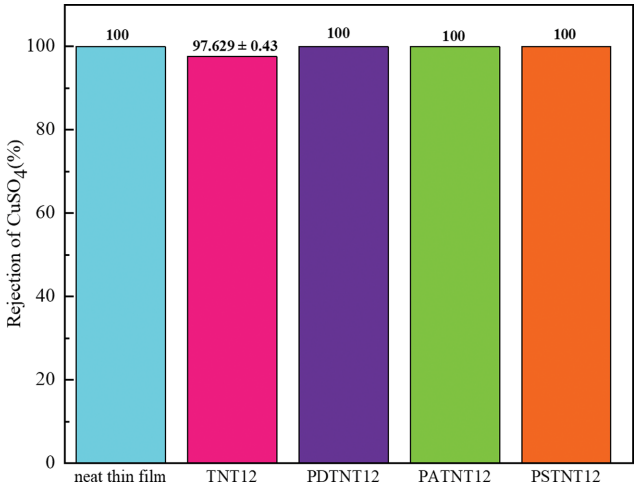


Fig. 11. Cu^{2+} rejection of the fabricated membranes.

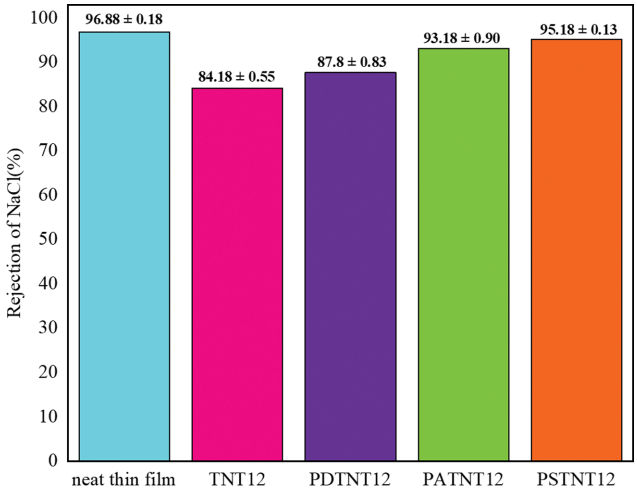


Fig. 12. Na^{+} rejection of the fabricated membranes.

water flux (Fig. 8). The accumulation of the ions on the surface of the membrane and the Donnan effect related to this phenomenon creates repulsion between the membrane surface and the hydrated ions and reduces the transfer rate of water through the membrane [3,82,93,94]. Furthermore, the dielectric exclusion effect makes hindrance for the ions in the solutions to pass through the nanotubes, which further lessens the permeation flux. In addition, the reduction in the inner diameter of the nanotubes makes more resistance for water molecules to pass through the membrane.

On the other hand, the feed solution permeation flux of the TFN membranes is generally higher than the neat TFC membrane; that can be related to the channeling effect of the well dispersed nanotubes in the PA layer, which facilitates the transfer of water [90,95]. The thickness of PA layer in NF membrane has great influence on the permeation flux where the thickness of active layer in TFN membranes may be lower due to the interaction between the nanotubes and MPD. Furthermore the accumulation of the NPs in the PA layer can create defects, which has a positive effect on the flux; the aggregation of NPs can further decrease the flux due to the blocking the entrance of the nanotube by another nanotube. It should further be considered that the nanotubes arranged in opposite direction can act as a barrier to water permeation [96]; the lower flux of PATNT12 membrane can be justified accordingly. In addition, the inner coating of the TNT nanotubes reduces the inner diameter of TNT nanotubes and the permeation flux of the membrane, even though the ion rejection can further be enhanced [97].

The rejections of Cu^{2+} and Na^{+} for the fabricated membranes are presented in Figs. 11-12, where the salt rejection of the membranes containing nanotubes is reduced compared to the neat membrane due to the trade-off between the permeability and rejection of the salts. On the other hand, the surface charges of the modified membranes (Donnan effect) increased because of the presence of the NPs in the polyamide layer [98-100]. The transfer rate of water and ions is further influenced by the nanotube diameter and hydrophilicity. The small size of the nanotube cavities can provide the energy barrier needed to reject the salts; therefore, the size of the nanotube is an important factor to determine the passage of the dissolved ions.

Referring to Figs. 11-12, the membranes showed more rejection for the copper ion. Furthermore, the rejections of the TFN membranes are generally less than TFC membrane; in case of TNT12 membrane, the reduction in ion rejection is more pronounced and that can be linked to the passage of ion through the nanotubes and the surface defects. Note that the mechanism of ion rejection in NF membrane is related to the ion size and the Donnan effect (ion repulsion) [98,101].

The size and charge of the ion (Donnan effect) have great effect on the rejection; therefore, copper, which is bigger in the hydrated form and has more charges, is rejected better than sodium. In addition, the functional groups (NH_2 and -COOH) on the surface of the PA layer make negative charges that repel the ions form the surface of the membrane; the addition of NPs can alter the surface charges of the membrane, which in case of the modified nanotubes, the pH_{PZC} test results showed that the modified nanotubes have

more negative charges than the neat TNT, which enhances the rejection of the ions compared to TNT12 membrane. On the other hand, the addition of nanotubes in the PA layer creates surface defects which improve the flux but lessen the rejection; the lower rejection of TFN membranes compared to TFC membrane can be justified accordingly.

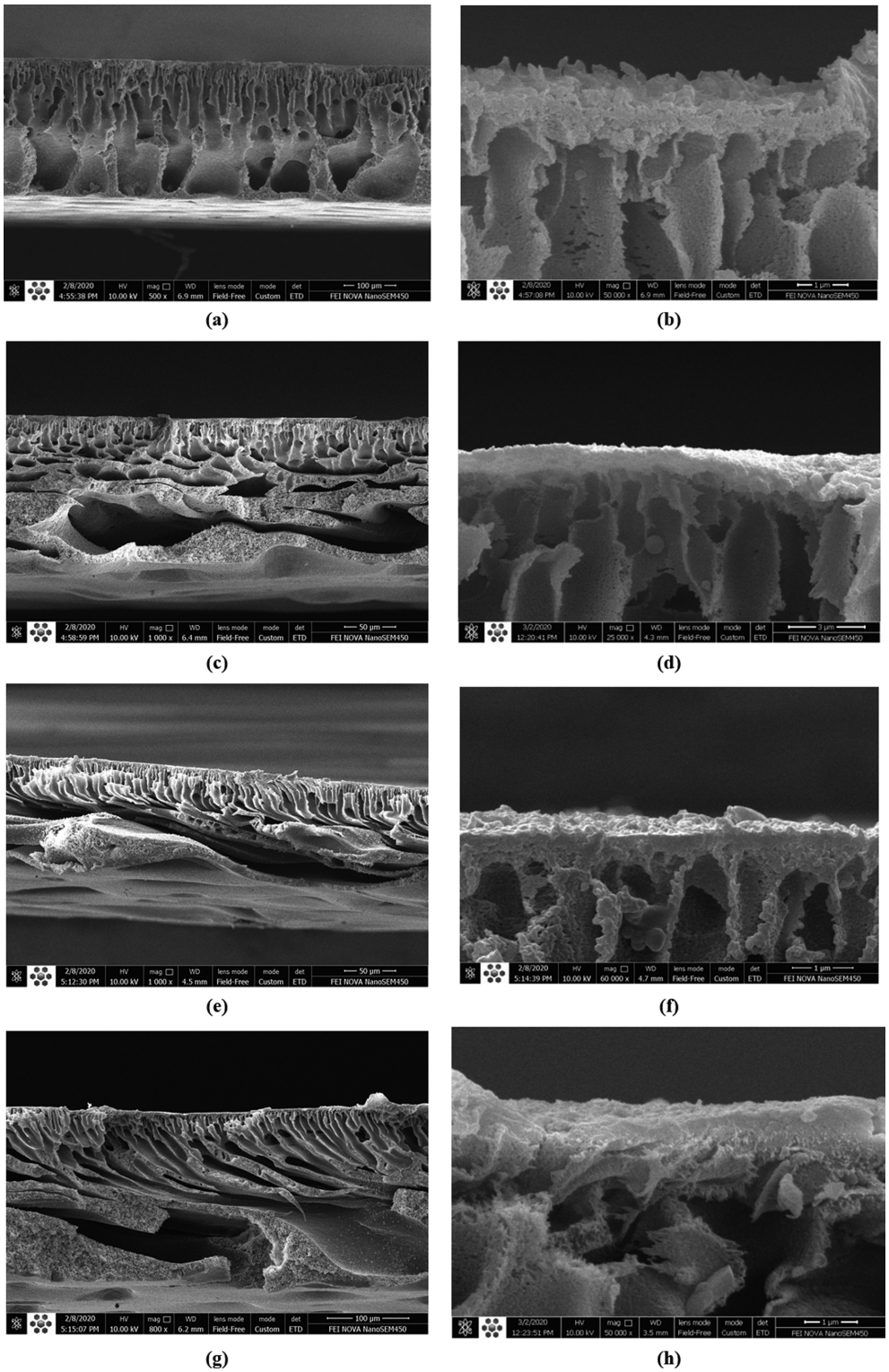


Fig. 13. FESEM images: (a) the cross section of neat TFC membrane, (b) skin layer of neat TFC membrane, (c) the cross section of 0.05 wt% TNT12, (d) skin layer of 0.05 wt% TNT12, (e) the cross section of 0.05 wt% PDTNT12, (f) skin layer of 0.05 wt% PDTNT12, (g) the cross section of 0.05 wt% PSTNT12, (h) skin layer of 0.05 wt% PSTNT12.

Furthermore, the inner coating of the nanotubes reduces the size and makes more spatial hindrance for the passage of the ions; the smaller inner diameter of the nanotubes and the functional groups in the structure of the coated polymers further intensifies the effect of dielectric exclusion phenomenon [62], which makes more resistance for the passage of the ions through the nanotubes.

The more negative charges of the TFN membranes that are related to the presence of the modified nanotubes can adsorb more cations and repel more anions. On the other hand, this phenomenon creates concentration polarization on the surface of the membrane where the accumulation of cations on the surface of the membrane decreases the negative surface charge density and pro-

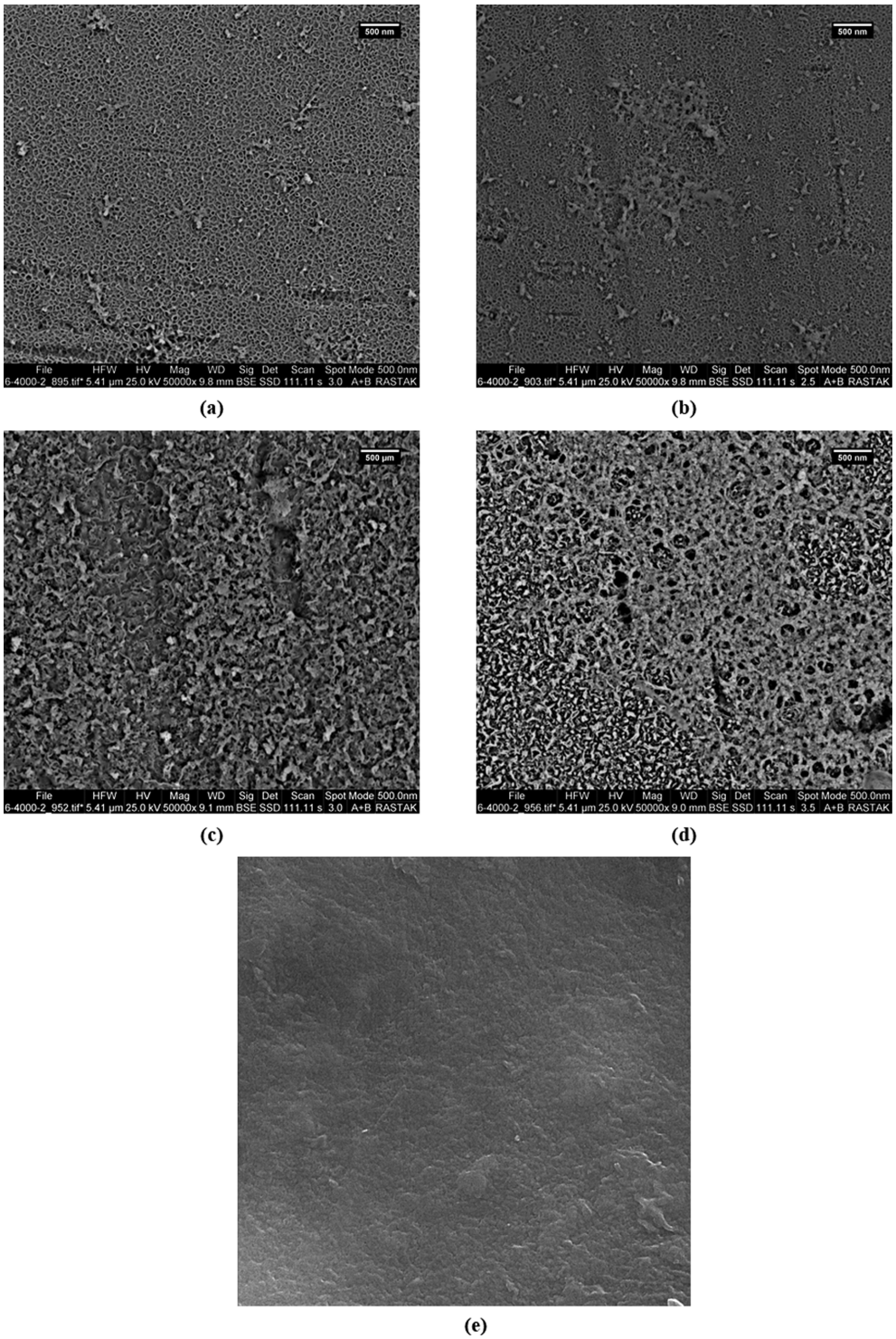


Fig. 14. Surface images of (a) neat TFC, (b) 0.05 wt% TNT12, (c) 0.05 wt% PDTNT12, (d) 0.05 wt% PSTNT12 thin film nanocomposite membranes, (e) PSf support membrane.

motes the diffusion of anions through the membrane and reduces the ion rejection [102]. The lower rejection of PDTNT12 membrane among the membranes containing modified nanotubes can be justified accordingly. Furthermore, the rejections of the membranes with the modified nanotubes are higher than TNT12 membrane; that can be related to the variation in inner diameter of the nanotubes and the spatial hindrance of the coated polymer.

2-4. SEM Analysis

The FESEM micrographs from the cross section and SEM micrographs form the surface of the selected membranes are presented in Figs. 13-14, respectively, where the surface of the membranes shows a ridge and valley structure that is related to the high solubility of MPD in n-hexane and its diffusion to the organic phase and reaction with TMC during the interfacial polymerization process [88,103,104].

Referring to Fig. 13(a), there are fingerlike macrovoids in the structure of the membrane sublayer that are related to the low concentration of the casting solution, which allows the coagulant (water) to penetrate in the structure of the membrane and create the voids. This structure reduces the resistance for the permeation of water through the membrane [103].

2-5. Contact Angle Measurement

The higher hydrophilicity makes water to pass through the membrane and improves the permeation flux [105,106]. The results of the contact angle measurements are shown in Fig. 15 where the addition of nanotubes generally improves the membrane hydrophilicity; that may be related to the adsorption of water by the hydrophilic nanotubes [97] and, after that, the penetration of water through the tubes. The coating of the inner surface of the nanotubes can increase the functional groups on the surface of the membrane [107,108], promote the penetration of water molecules through the tubes and improve the hydrophilic character and water permeation of the membrane, as shown in Fig. 8.

2-6. AFM Analysis

Fig. S6 and Table S1 present the images from the membranes' surface and the data of the roughness parameters, RMS and R_a, respectively, where the surface of the prepared membranes shows rough ridge-valley morphology that is the characteristic of polyamide TFC membranes, synthesized through the IP process [109, 110]. The surface roughness of the membranes containing nano-

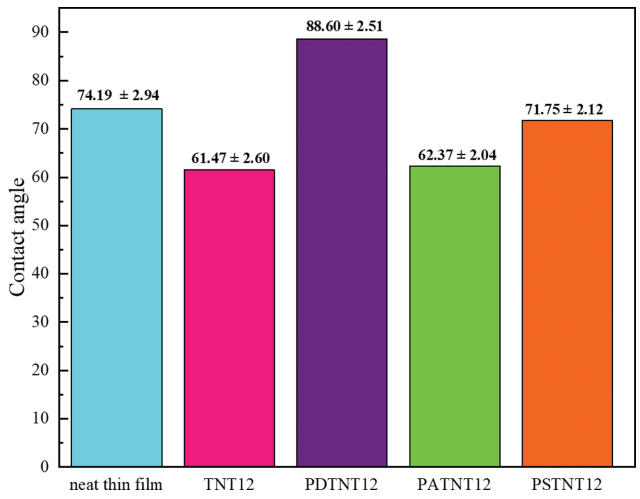


Fig. 15. Contact angle of thin film nanocomposite membranes with modified/unmodified nanotubes.

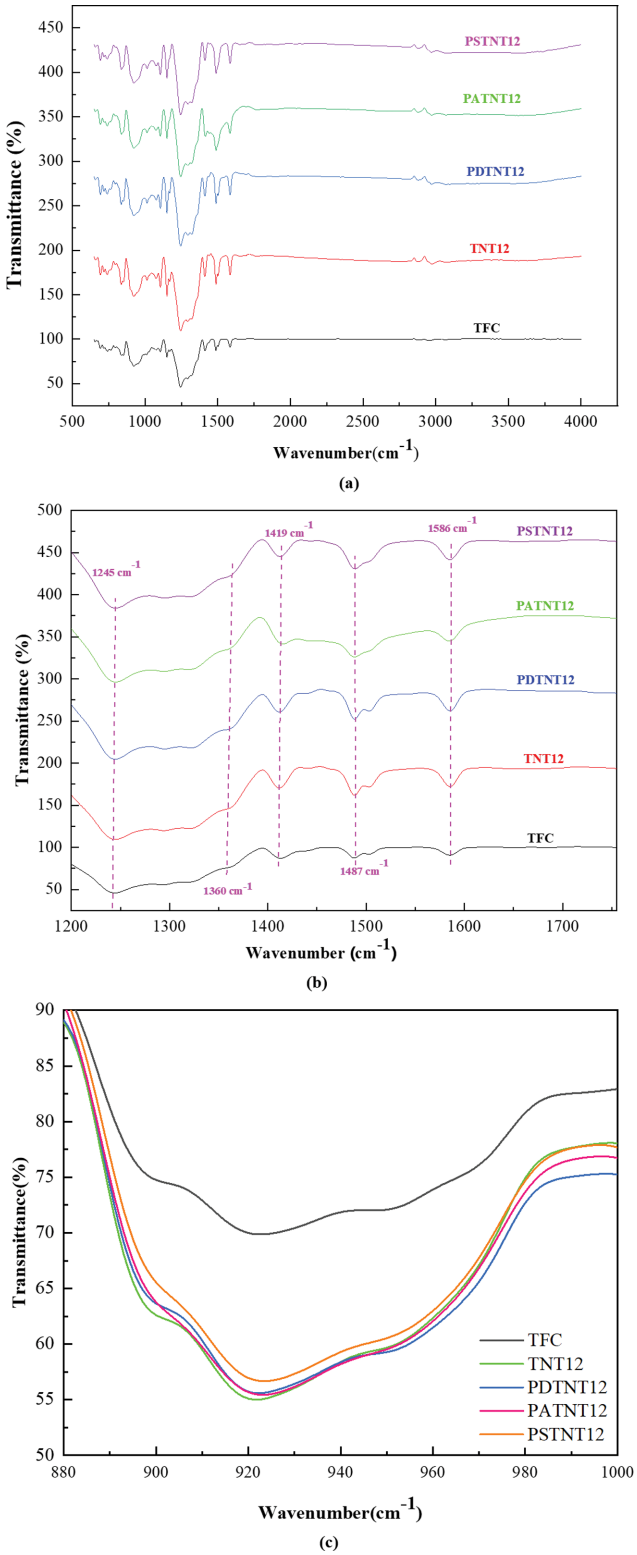


Fig. 16. ATR-FTIR spectroscopy of TFC/TFN membranes, (a) in the range of 640-4,000 cm^{-1}, (b) in the range of 1,200-1,800 cm^{-1}, (c) in the range of 880-1,000 cm^{-1}.

Table 2. Comparison of TFN membrane synthesized in this study and those fabricated in other research

Membrane fabrication method	Membrane process	Feed solution & concentration	NPs	Pure water flux (L m^{-2} h^{-1})	Rejection (%)	Reference
IP	NF	500 ppm $CuSO_4$ 200 ppm NaCl	PSTNT12	26.13	100 95.18	This work
IP	FO	10 ppm Cd^{2+} 10 ppm Pb^{2+}	TNT-Fe_3O_4	2.82	98.8 99.8	[120]
IP	RO	2,000 ppm NaCl	GO/PVA	12.24	96.28	[121]
Chemical crosslinking	NF	500 ppm $MgCl_2$ 500 ppm $MgSO_4$ 500 ppm Na_2SO_4 500 ppm NaCl 500 ppm $MgCl_2$ 500 ppm $MgSO_4$ 500 ppm Na_2SO_4 500 ppm NaCl	(MWCNTs) GO 	276.91 393.46 	90 80 25 30 86 78 20 25	[122]
IP	RO	2,000 ppm NaCl	UiO-66-NH_2 nanoparticles	55	99.1	[123]
IP	RO	2,000 ppm NaCl	TiO_2 nanoparticles	24.32	97.7	[124]
IP	FO	1,160 ppm NaCl	NH_2-TNTs	20.79	94.1	[38]
Self-assembly	NF	0.12 ppm NaCl 10 ppm $CuSO_4$ 50 ppm dye	TiO_2 nanorods among graphene sheets	29.6	41.2 93.2 99.7	[125]
IP	NF	2,000 ppm Na_2SO_4	β zeolite	81.22	97.59	[126]

tubes can be more than neat TFC membrane because of the presence of the nanotubes and their aggregation on the PA layer of the membrane; this phenomenon can increase the contact angle and further enhance the dielectric repulsion of the ions and improve the ion rejection.

In this study, the TFN membrane shows lower roughness that can be related to the interaction between the TNTs and MPD, which slows the diffusion of MPD to the aqueous/organic interface (reaction zone) [111,112]. It is further possible that the hydrogen bonds in the nanotubes lead to the formation of a denser layer [112]. The lower surface roughness can reduce the water permeation as was reported elsewhere [111,113,114].

2-7. The ATR-FTIR Spectroscopy of TFC/TFN Membranes

The ATR-FTIR spectroscopy of TFC and TFN membranes, containing modified/unmodified TNT12 is shown in full range in Fig. 16(a) and in the range of 1,200-1,800 cm^{-1} in Fig. 16(b), where the band at 1,586 cm^{-1} is related to PSf substrate [115]. The peak at 1,360 cm^{-1} is attributed to the stretching of C=O (amine I) [116]. In addition, the peaks related to the plane bending of N-H (amine II) and stretching vibration of C-N (amine III) are shown at 1,487 cm^{-1} and 1,245 cm^{-1} [117], respectively; the band related to the bending vibration of CH_2 can be observed at 1,419 cm^{-1} [118]. Therefore the peaks related to the polyamide layer were confirmed.

In Fig. 16(c), the FTIR spectra for the fabricated membranes are shown in the range of 880-1,000 cm^{-1} where the peak at 920-950 cm^{-1} is related to the unreacted acyl chloride groups in TMC [119]; thus, this peak can be considered as a criterion for the incomplete reaction between MPD and TMC (degree of crosslinking). It is interesting that the addition of nanotubes reduced the degree of crosslinking that can be related to the interaction of MPD and nanotubes, which reduces the concentration of MPD in the reaction zone, as was explained before.

2-8. Comparison of the Results with other Research

The performance of PSTNT12 membrane was compared with other research in terms of the pure water flux and rejection and the results are shown in Table 2.

Soo et al. [120] used a method to enhance the performance of TFN membrane in heavy metal ion separation through blending TNT-Fe_3O_4 in the PSf substrate of the membrane to improve the hydrophilicity and increase the water flux from 1.63 L m^{-2} h^{-1} to 2.82 L m^{-2} h^{-1} (73% enhancement). Ng et al. [121] proposed a new method for TFN membrane fabrication where a layer of polyvinyl alcohol/graphene oxide is sandwiched between the PA layer and the substrate. The fabricated membranes showed improved surface hydrophilicity, NaCl rejection and antifouling properties. To improve the performance of TFN membranes, Valamohammadi et al. [122] at first modified the hydrolyzed polyacrylonitrile sublayer by multi-walled carbon nanotubes and graphene oxide and then coated hyperbranched polyethyleneimine on the sublayer and crosslinked by glutaraldehyde. They reported the pure water flux of TFN membranes containing CNT and GO improved by 38% and 64%, respectively, compared to the TFC membrane. They claimed that the higher permeation is related to the sublayer hydrophilicity, tubular structure of CNTs and channels between

the GO nanosheets. Zhao et al. [123] blended the UiO-66-NH_2 metal organic frameworks (MOFs) with the size of ~100 nm into the PA layer of RO membranes through spray assisted pre-deposition method and claimed that the porous structure, suitable size of the triangular opening and the hydrophilic nature of MOFs can affect the surface hydrophilicity and degree of crosslinking of TFN membranes. Furthermore, the MOFs can create preferential pathways for the transport of water across the membrane structure. The water permeation of MOFs modified membrane increased by 50%, while the rejection was the same as TFC membrane. To overcome the aggregation and weak compatibility of NPs with the polymer matrix, Khorshidi et al. [124] proposed the simultaneous synthesis and surface functionalization of TiO_2 NPs by application of biphasic solvothermal reaction and, then, used the stable suspension of TiO_2 NPs in the fabrication of TFN membrane. Emadzadeh et al. [38] synthesized TFN membranes containing amine-functionalized TNTs for forward osmosis process, which the membranes showed water flux improvement without any decline in the salt rejection. Liu et al. [125] synthesized TiO_2 nanorod from anatase TiO_2 nanoparticles by hydrothermal method and graphene oxide sheets by the modified Hummer method and then synthesized GO-TiO_2 nanorod composite by the hydrothermal method at 120 °C. The composite was inserted on the cellulose acetate mat by vacuum filtration method and used in the separation process; the results showed high flux and rejection, especially for dyes. Borjigin et al. [126] synthesized polyamide thin film nanocomposite membranes by incorporating β-zeolite at different concentrations, which improved the water permeability to 81.22 L m^{-2} h^{-1} because of its porous structure and tiny-sized pores that act as the channel for water and barrier for ions.

CONCLUSIONS

The effects of internal surface modification of titanate nanotubes (TNTs) on the performance of nanofiltration membranes were studied. At first, TNTs were synthesized through hydrothermal method and then their inner surface was coated with different polymers through a novel in-situ polymerization process to alter the chemistry and size of the inner surface of the nanotubes. Finally, the TFN/TFC membranes were synthesized and their characteristics in terms of permeation flux and rejection of monovalent (Na^+) and divalent ions (Cu^{2+}) were studied. According to the FTIR, BET, XRD and TEM tests, it can be claimed that the inner coating of the nanotubes was successful without any noticeable change in the shape/structure of the nanotubes. The internal coating of the nanotubes can control the passage of the ions through the polyamide layer of the membrane by decreasing the inner diameter of the nanotubes and creating more repulsion forces because of the steric hindrance and size exclusion effect. The fabricated TFN/TFC membranes were characterized by SEM, contact angle, permeation flux and Cu^{2+}/Na^+ ion rejection tests. Generally, the permeation flux of TFN membranes containing unmodified/modified TNTs was improved compared to TFC membrane; that can be related to the channeling effect of TNTs. On the other hand, the TFN membranes containing modified TNTs presented lower permeation flux; that may be linked to the inner coating and less space for the water transport, even though the inner surface modification can make more hydrophilic groups in the structure of the membrane and more water adsorption.

The rejection of the ions for the membrane containing unmodified TNT is lower than TFC membrane that is linked to the passage of the ions through the nanotubes, but it is interesting that the inner surface modification of TNT improved the rejection that is related to the size exclusion effect and steric hindrance of the coating, making more repulsion for the ions to pass through the nanotubes. Among the fabricated membranes, the membrane containing polystyrene coated TNT showed the best trade-off between permeation and rejection, which the permeation flux was ~70% higher than TFC membranes, whereas the ion rejection was the same. Through blending modified TNTs in the membrane structure, the mass transfer path for the water molecules may be longer in case of passing through the nanotubes, but it seems that this path makes less resistance compared to the PA layer.

ACKNOWLEDGEMENT

The authors gratefully acknowledge the financial support from the Babol Noshirvani University of Technology of Iran through research Grant No (BNUT/955150012/97).

NOMENCLATURE

A	: effective membrane area
AFM	: atomic force microscopy
APS	: ammonium peroxydisulfate
BET	: Brunauer-Emmett-Teller
CA	: contact angle
CSA	: camphorsulfonic acid
DI	: deionized water
FESEM	: field emission scanning electron microscope
FTIR	: Fourier-transform infrared spectroscopy
IP	: interfacial polymerization
l	: membrane thickness
MPD	: m-phenylenediamine
NF	: nanofiltration
NMP	: N-methyl-2-pyrrolidone
NPs	: nanoparticles
PA	: polyamide
PATNT12	: TNT12 coated with polyaniline
PDTNT12	: TNT12 coated with polydopamine
PSf	: polysulfone
PSTNT12	: TNT12 coated with polystyrene
PVP	: polyvinylpyrrolidone
Q	: permeation flow rate
r_m	: mean pore size
RO	: reverse osmosis
SEM	: scanning electron microscope
TEA	: triethyleneamine
TEM	: transmission electron microscope
TFC	: thin film composite
TFN	: thin film nanocomposite
TMC	: trimesoyl chloride

TNT12 : titanate nanotubes
UF : ultrafiltration
v_m : total volume of the pores
XRD : X-ray powder diffraction
ε : porosity
ρ_w : water density
ρ_p : polymer density
η : water viscosity

SUPPORTING INFORMATION

Additional information as noted in the text. This information is available via the Internet at http://www.springer.com/chemistry/journal/11814.

REFERENCES

1. S. P. Dharupaneedi, S. K. Nataraj, M. Nadagouda, K. R. Reddy, S. S. Shukla and T. M. Aminabhavi, *Sep. Purif. Technol.*, **210**, 850 (2019).
2. P. S. Goh, T. W. Wong, J. W. Lim, A. F. Ismail and N. Hilal, *Innovation strategies in environmental science*, C. M. Galanakis (Ed.), Elsevier (2020).
3. M. Peydayesh, S. Bolisetty, T. Mohammadi and R. Mezzenga, *Langmuir*, **35**, 4161 (2019).
4. S. Bolisetty, M. Peydayesh and R. Mezzenga, *Chem. Soc. Rev.*, **48**, 463 (2019).
5. D. Cohen-Tanugi, R. K. McGovern, S. H. Dave, J. H. Lienhard and J. C. Grossman, *Energy Environ. Sci.*, **7**, 1134 (2014).
6. R. Hu, R. Zhang, Y. He, G. Zhao and H. Zhu, *J. Membr. Sci.*, **564**, 813 (2018).
7. L. Shen, X. Zhang, J. Zuo and Y. Wang, *J. Membr. Sci.*, **534**, 46 (2017).
8. L. Shen, F. Wang, L. Tian, X. Zhang, C. Ding and Y. Wang, *J. Membr. Sci.*, **563**, 284 (2018).
9. Z. Jiang, J. Miao, Y. He, K. Tu, S. Chen, R. Zhang, L. Zhang and H. Yang, *RSC Adv.*, **9**, 10796 (2019).
10. F. Aghili, A. A. Ghoreyshi, B. Van der Bruggen and A. Rahimpour, *Process Saf. Environ. Prot.*, **151**, 244 (2021).
11. Z. Zhang, G. Kang, H. Yu, Y. Jin and Y. Cao, *Desalination*, **466**, 16 (2019).
12. M. H. Tajuddin, N. Yusof, N. Abdullah, M. N. Z. Abidin, W. N. W. Salleh, A. F. Ismail, T. Matsuura, N. H. H. Hairom and N. Misdan, *J. Taiwan Inst. Chem. Eng.*, **97**, 1 (2019).
13. B. Liu, S. Wang, P. Zhao, H. Liang, W. Zhang and J. Crittenden, *Appl. Surf. Sci.*, **435**, 415 (2018).
14. M. He, T. Li, M. Hu, C. Chen, B. Liu, J. Crittenden, L.-Y. Chu and H. Y. Ng, *Sep. Purif. Technol.*, **230**, 115855 (2020).
15. H. B. Li, H. X. Zhang, X. H. Qin and W. Y. Shi, *Appl. Surf. Sci.*, **407**, 260 (2017).
16. W. J. Lau, A. Ismail, N. Misdan and M. Kassim, *Desalination*, **287**, 190 (2011).
17. M. A. Kamaruddin, N. Ismail, U. N. Osman and R. Alrozi, *Appl. Water Sci.*, **9**, 141 (2019).
18. X. Liu, B. Jiang, X. Yin, H. Ma and B. S. Hsiao, *Sep. Purif. Technol.*, **233**, 115976 (2020).
19. M. Bost, S. Houdart, M. Oberli, E. Kalonji, J. F. Huneau and I. Margaritis, *J. Trace. Elem. Med. Biol.*, **35**, 107 (2016).
20. F. Yan, H. Chen, Y. Lü, Z. Lü, S. Yu, M. Liu and C. Gao, *J. Membr. Sci.*, **513**, 108 (2016).
21. Y. Liu, X. Wang, X. Gao, J. Zheng, J. Wang, A. Volodin, Y. F. Xie, X. Huang, B. Van der Bruggen and J. Zhu, *J. Membr. Sci.*, **596**, 117717 (2020).
22. J. R. Werber, C. O. Osuji and M. Elimelech, *Nat. Rev. Mater.*, **1**, 16018 (2016).
23. P. Lu, W. Li, S. Yang, Y. Liu, Q. Wang and Y. Li, *Sep. Purif. Technol.*, **220**, 231 (2019).
24. T. Wang, H. Qiblawey, S. Judd, A. Benamor, M. S. Nasser and A. Mohammadian, *J. Membr. Sci.*, **552**, 222 (2018).
25. X. Hao, S. Gao, J. Tian, Y. Sun, F. Cui and C. Y. Tang, *Environ. Sci. Technol.*, **53**, 4371 (2019).
26. P. G. Ingole, W. K. Choi, G. B. Lee and H. K. Lee, *Desalination*, **403**, 12 (2017).
27. X. Song, B. Gan, Z. Yang, C. Y. Tang and C. Gao, *J. Membr. Sci.*, **582**, 342 (2019).
28. Y. Qi, L. Zhu, X. Shen, A. Sotto, C. Gao and J. Shen, *Sep. Purif. Technol.*, **222**, 117 (2019).
29. M. Guo, S. Wang, K. Gu, X. Song, Y. Zhou and C. Gao, *J. Membr. Sci.*, **569**, 83 (2019).
30. M. I. Baig, P. G. Ingole, J.-d. Jeon, S. U. Hong, W. K. Choi, B. Jang and H. K. Lee, *Desalination*, **451**, 59 (2019).
31. H. Li, W. Shi, H. Zhu, Y. Zhang, Q. Du and X. Qin, *Fibers Polym.*, **17**, 836 (2016).
32. M. Liu, Z. Jia, D. Jia and C. Zhou, *Prog. Polym. Sci.*, **39**, 1498 (2014).
33. M. H. Razali, N. A. Ismail and K. A. Mat Amin, *Int. J. Biol. Macromol.*, **153**, 1117 (2020).
34. J. S. Appasamy, J. C. Kurnia and M. K. Assadi, *Sol. Energy*, **196**, 80 (2020).
35. L. Bautista-Patacsil, J. P. L. Lazarte, R. C. Dipasupil, G. Y. Pasco, R. C. Eusebio, A. Orbecido and R. Doong, *J. Environ. Chem. Eng.*, **8**, 103063 (2020).
36. M. M. Momeni, *Appl. Surf. Sci.*, **357**, 160 (2015).
37. B. Rajaeian, A. Rahimpour, M. O. Tade and S. Liu, *Desalination*, **313**, 176 (2013).
38. D. Emadzadeh, W. J. Lau, M. Rahbari-Sisakht, H. Ilbeygi, D. Rana, T. Matsuura and A. F. Ismail, *Chem. Eng. J.*, **281**, 243 (2015).
39. P. Kedchaikulrat, I. F. J. Vankelecom, K. Faungnawakij and C. Klaysom, *Colloid Surf. A-Physicochem. Eng. Asp.*, **601**, 125046 (2020).
40. R. Kumar, M. Ahmed, G. Bhadrachari, S. Al-Muqahwi and J. P. Thomas, *J. Environ. Chem. Eng.*, **9**, 105722 (2021).
41. K. Szymański, D. Darowna, P. Sienkiewicz, M. Jose, K. Szymańska, M. Zgrzebnicki and S. Mozia, *J. Water Process. Eng.*, **33**, 101098 (2020).
42. G. Liu, K. Han, Y. Zhou, H. Ye, X. Zhang, J. Hu and X. Li, *ACS Sustain. Chem. Eng.*, **6**, 6256 (2018).
43. V. Giel, M. Perchacz, J. Kredatusová and Z. Pientka, *Nanoscale Res. Lett.*, **12**, 3 (2017).
44. M. Delavar, G. Bakeri, M. Hosseini and N. Nabian, *Can. J. Chem. Eng.*, **98**, 1558 (2020).
45. I. Wan Azelee, P. S. Goh, W. J. Lau, A. F. Ismail, M. Rezaei-DashtArzhandi, K. C. Wong and M. N. Subramaniam, *Desalination*, **409**, 163 (2017).
46. T. A. Hilder, D. Gordon and S.-H. Chung, *Small*, **5**, 2183 (2009).
47. Y. Wei, Y. Zhu and Y. Jiang, *Chem. Eng. J.*, **356**, 915 (2019).

48. R. Das, M. E. Ali, S. B. A. Hamid, S. Ramakrishna and Z. Z. Chowdhury, *Desalination*, **336**, 97 (2014).
49. R. Das, S. B. Abd Hamid, M. E. Ali, A. F. Ismail, M. S. M. Annuar and S. Ramakrishna, *Desalination*, **354**, 160 (2014).
50. V. R. K. Velpula, T. Ketike, G. Paleti, S. R. R. Kamaraju and D. R. Burri, *Catal. Lett.*, **150**, 95 (2020).
51. A. Benamor, M. Nasser, M. H. El-Naas and H. Qiblawey, *Iop Conf. Ser. Mater. Sci. Eng. (discontin.)*, **634**, 012048 (2019).
52. M. N. Subramaniam, P. S. Goh, N. Abdullah, W. J. Lau, B. C. Ng and A. F. Ismail, *J. Nanopart. Res.*, **19**, 220 (2017).
53. V. Elumalai, T. Deenadhayalan, A. Kathleen Asitha, D. Joel Kirubhakaran and D. Sangeetha, *SN Appl. Sci.*, **1**, 348 (2019).
54. S. Brunauer, P. H. Emmett and E. Teller, *JACS*, **60**, 309 (1938).
55. G. Bakeri and Z. Fallahnejad, *Desalination Water Treat.*, **62**, 57 (2017).
56. S. N. Wan Ikhsan, N. Yusof, F. Aziz, N. Misdan, A. F. Ismail, W.-J. Lau, J. Jaafar, W. N. Wan Salleh and N. H. Hayati Hairom, *Sep. Purif. Technol.*, **199**, 161 (2018).
57. S. Mohsenpour, S. Leaper, J. Shokri, M. Alberto and P. Gorgojo, *J. Membr. Sci.*, **641**, 119924 (2021).
58. M. Delavar, G. Bakeri and M. Hosseini, *Chem. Eng. Res. Des.*, **120**, 240 (2017).
59. M. Hezarjaribi, G. Bakeri, M. Sillanpää, M. J. Chaichi and S. Akbari, *J. Water Process. Eng.*, **37**, 101401 (2020).
60. R. S. Hebbar, A. M. Isloor and A. F. Ismail, *Membrane characterization*, N. Hilal, A. F. Ismail, T. Matsuura, D. Oatley-Radcliffe (Eds.), Elsevier (2017)
61. A. W. Neumann and R. J. Good, *Surface and colloid science: Volume 11: Experimental methods*, R. J. Good, R. R. Stromberg (Eds.), Springer US, Boston, MA (1979)
62. S. Gholami, J. López, A. Rezvani, V. Vatanpour and J. L. Cortina, *Chem. Eng. J.*, **384**, 123348 (2020).
63. X. Cao, H. Liu, X. Yang, J. Tian, B. Luo and M. Liu, *Compos. Sci. Technol.*, **191**, 108071 (2020).
64. W. F. Monteiro, M. O. Vieira, E. F. Laschuk, P. R. Livotto, S. M. O. Einloft, M. O. de Souza and R. A. Ligabue, *J. CO_2 Util.*, **37**, 20 (2020).
65. N. Seddaoui and A. Amine, *LWT*, **122**, 109045 (2020).
66. R. Zheng, S. Wang, Y. Tian, X. Jiang, D. Fu, S. Shen and W. Yang, *ACS Appl. Mater. Interfaces*, **7**, 15876 (2015).
67. S. S. Ghasemi, E. Mohammadnia, M. Hadavifar and H. Veisi, *AUT J. of Civil Engineering*, **4**, 315 (2020).
68. S. Acter, M. L. P. Vidallon, S. Crawford, R. F. Tabor and B. M. Teo, *Part. Part. Syst. Charact.*, **37**, 2000166 (2020).
69. X. Yu, H. Fan, Y. Liu, Z. Shi and Z. Jin, *Langmuir*, **30**, 5497 (2014).
70. Y. Cheng, A. Barras, S. Lu, W. Xu, S. Szunerits and R. Boukherroub, *Sep. Purif. Technol.*, **236**, 116240 (2020).
71. H. Yang, H. Chen, L. Cao, H. Wang, W. Deng, Y. Tan and Q. Xie, *Talanta*, **212**, 120797 (2020).
72. H. Xu, D. Zheng, F. Liu, W. Li and J. Lin, *J. Mater. Chem. A*, **8**, 5853 (2020).
73. S. G. Pawar, S. L. Patil, M. A. Chougule, A. T. Mane, D. M. Jundale and V. B. Patil, *Int. J. Polym. Mater. Po*, **59**, 777 (2010).
74. L. Li, H. Song, Q. Zhang, J. Yao and X. Chen, *J. Power Sources*, **187**, 268 (2009).
75. A. Mahudeswaran, J. Vivekanandan and P. S. Vijayanand, *Mater. Today: Proc.*, **47**, 2154 (2021).
76. A. Mahudeswaran, P. S. Vijayanand, J. Vivekanandan and J. Chandrasekaran, *Mater. Today: Proc.*, **45**, 3409 (2021).
77. S. Sohrabi, M. Keshavarz Moraveji and D. Iranshahi, *J. Mol. Liq.*, **343**, 116979 (2021).
78. O. Pereao, K. Laatikainen, C. Bode-Aluko, I. Kochnev, O. Fatoba, A. N. Nechaev and L. Petrik, *Sep. Purif. Technol.*, **233**, 116059 (2020).
79. L. Chen, H. Ji, J. Qi, T. Huang, C.-C. Wang and W. Liu, *Chem. Eng. J.*, **406**, 126877 (2021).
80. X. Zhao, Z. Cai, T. Wang, S. E. O'Reilly, W. Liu and D. Zhao, *Appl. Catal. B.*, **187**, 134 (2016).
81. J. Ma, F. Li, T. Qian, H. Liu, W. Liu and D. Zhao, *Chem. Eng. J.*, **315**, 191 (2017).
82. A. Saeedi-Jurkuyeh, A. J. Jafari, R. R. Kalantary and A. Esrafili, *React. Funct. Polym.*, **146**, 104397 (2020).
83. M. S. Rezaeian, S. M. Mousavi, E. Saljoughi and H. A. Akhlaghi Amiri, *Desalination*, **474**, 114194 (2020).
84. Q. Yang, Y. Su, C. Chi, C. T. Cherian, K. Huang, V. G. Kravets, F. C. Wang, J. C. Zhang, A. Pratt, A. N. Grigorenko, F. Guinea, A. K. Geim and R. R. Nair, *Nat. Mater.*, **16**, 1198 (2017).
85. L. Paseta, J. M. Luque-Alled, M. Malankowska, M. Navarro, P. Gorgojo, J. Coronas and C. Téllez, *Sep. Purif. Technol.*, **247**, 116995 (2020).
86. C. Echaide-Górriz, S. Sorribas, C. Téllez and J. Coronas, *RSC Adv.*, **6**, 90417 (2016).
87. W. C. J. Park, S.-H. Kim, B.-H. Chun, J. Bang and K.-B. Lee, *Desalination Water Treat.*, **15**, 198 (2012).
88. S. Seyyed Shahabi, N. Azizi, V. Vatanpour and N. Yousefimehr, *Sep. Purif. Technol.*, **235**, 116134 (2020).
89. J. María Arsuaga, A. Sotto, G. del Rosario, A. Martínez, S. Molina, S. B. Teli and J. de Abajo, *J. Membr. Sci.*, **428**, 131 (2013).
90. H. D. Lee, H. W. Kim, Y. H. Cho and H. B. Park, *Small*, **10**, 2653 (2014).
91. H.-R. Chae, J. Lee, C.-H. Lee, I.-C. Kim and P.-K. Park, *J. Membr. Sci.*, **483**, 128 (2015).
92. Y. Zhang, H. Ruan, C. Guo, J. Liao, J. Shen and C. Gao, *Sep. Purif. Technol.*, **234**, 116017 (2020).
93. B. M. Jun, J. Cho, A. Jang, K. Chon, P. Westerhoff, Y. Yoon and H. Rho, *Sep. Purif. Technol.*, **247**, 117026 (2020).
94. M. Peydayesh, T. Mohammadi and S. K. Nikouzad, *J. Membr. Sci.*, **611**, 118205 (2020).
95. D. L. Oatley, L. Llenas, R. Pérez, P. M. Williams, X. Martínez-Lladó and M. Rovira, *Adv. Colloid Interface Sci.*, **173**, 1 (2012).
96. M. Yu, H. H. Funke, J. L. Falconer and R. D. Noble, *Nano Lett.*, **9**, 225 (2009).
97. H. Zarrabi, M. E. Yekavalangi, V. Vatanpour, A. Shockravi and M. Safarpour, *Desalination*, **394**, 83 (2016).
98. H. Wu, B. Tang and P. Wu, *J. Phys. Chem. C.*, **114**, 16395 (2010).
99. M. Xu, X. Feng, Z. liu, X. Han, J. Zhu, J. Wang, B. V. d. Bruggen and Y. Zhang, *Sep. Purif. Technol.*, **275**, 119150 (2021).
100. X. Gao, P. Li, Z. Gu, Q. Xiao, S. Yu and L. a. Hou, *J. Membr. Sci.*, 119711 (2021).
101. R. Hu, Y. He, C. Zhang, R. Zhang, J. Li and H. Zhu, *J. Mater. Chem. A*, **5**, 25632 (2017).
102. J. Nambikkattu, N. J. Kaleekkal and J. P. Jacob, *Environ. Sci. Pollut. Res.*, **28**, 11915 (2021).

103. M. Amini, M. Seifi, A. Akbari and M. Hosseinifard, *Polyhedron*, **179**, 114362 (2020).
104. C. Y. Tang, Q. S. Fu, C. S. Criddle and J. O. Leckie, *Environ. Sci. Technol.*, **41**, 2008 (2007).
105. Y. Rahimi-Kashkouli, M. Rahbari-Sisakht and A. Ghadami Jadval Ghadam, *Environ. Sci. Water Res. Technol.*, **6**, 715 (2020).
106. F. Asempour, D. Emadzadeh, T. Matsuura and B. Kruczek, *Desalination*, **439**, 179 (2018).
107. S. Bandehali, F. Parvizian, A. R. Moghadassi, S. M. Hosseini and J. N. Shen, *J. Polym. Res.*, **27**, 94 (2020).
108. Z. Zhou, J. Y. Lee and T.-S. Chung, *Chem. Eng. J.*, **249**, 236 (2014).
109. H. Mahdavi and A. Rahimi, *Desalination*, **433**, 94 (2018).
110. W. Choi, J. Choi, J. Bang and J. H. Lee, *ACS Appl. Mater. Interfaces*, **5**, 12510 (2013).
111. H. R. Chae, C. H. Lee, P. K. Park, I. C. Kim and J. H. Kim, *J. Membr. Sci.*, **525**, 99 (2017).
112. S. F. Seyedpour, A. Rahimpour, A. A. Shamsabadi and M. Soroush, *Chem. Eng. Res. Des.*, **139**, 321 (2018).
113. Y. Song, P. Sun, L. L. Henry and B. Sun, *J. Membr. Sci.*, **251**, 67 (2005).
114. Y. Yang, X. Yang, W. Yang, S. Li, J. Xu and Y. Jiang, *Nanoscale Res. Lett.*, **9**, 537 (2014).
115. R. Xu, F. Gao, Y. Wu, L. Ding, D. Chen, T. Liu, Y. Yu, W. Zhuo, Z. Chen, Y. Zhang, Y. Sun, F. Yang, J. Chen, Y. Cao, J. Kang, Z. Zheng and M. Xiang, *Sep. Purif. Technol.*, **281**, 119884 (2022).
116. C. Geng, P. Huang, F. Zhao, H. Dong, H. Niu, Y. Zhou, J. Shen and J. Zhang, *J. Membr. Sci.*, **637**, 119637 (2021).
117. F. F. Chen, T. Su, X. T. Zhao, J. F. Pan and L. F. Liu, *J. Membr. Sci.*, **637**, 119625 (2021).
118. Y. Qin, S. Yu, Q. Zhao, G. Kang, H. Yu, Y. Jin and Y. Cao, *Desalination*, **499**, 114840 (2021).
119. J. Lee, R. Wang and T.-H. Bae, *J. Membr. Sci.*, **583**, 70 (2019).
120. K. W. Soo, K. C. Wong, P. S. Goh, A. F. Ismail and N. Othman, *J. Water Process. Eng.*, **38**, 101591 (2020).
121. Z. C. Ng, W. J. Lau and A. F. Ismail, *Desalination*, **496**, 114538 (2020).
122. E. Valamohammadi, F. Behdarvand, M. A. Tofighy and T. Mohammadi, *Sep. Purif. Technol.*, **242**, 116826 (2020).
123. D. L. Zhao, W. S. Yeung, Q. Zhao and T.-S. Chung, *J. Membr. Sci.*, **604**, 118039 (2020).
124. B. Khorshidi, T. Thundat, B. Fleck and M. Sadrzadeh, *RSC Adv.*, **5**, 54985 (2015).
125. Y. Liu, Z. Yu, Y. Peng, L. Shao, X. Li and H. Zeng, *Chem. Phys. Lett.*, **749**, 137424 (2020).
126. B. Borjigin, L. Liu, L. Yu, L. Xu, C. Zhao and J. Wang, *J. Environ. Sci.*, **98**, 77 (2020).

Supporting Information

Performance of TFN nanofiltration membranes through embedding internally modified titanate nanotubes

Zeynab Fallahnejad*, Gholamreza Bakeri*,,†, and Ahmad Fauzi Ismail*****

*Chemical Engineering Faculty, Babol Noshirvani University of Technology, Babol, Iran
**Advanced Membrane Research Lab, Babol Noshirvani University of Technology, Babol, Iran
***Advanced Membrane Technology Research Centre (AMTEC), Universiti Teknologi Malaysia, 81310 Skudai, Johor Darul Takzim, Malaysia
(*Received 29 August 2021 • Revised 28 November 2021 • Accepted 2 December 2021*)

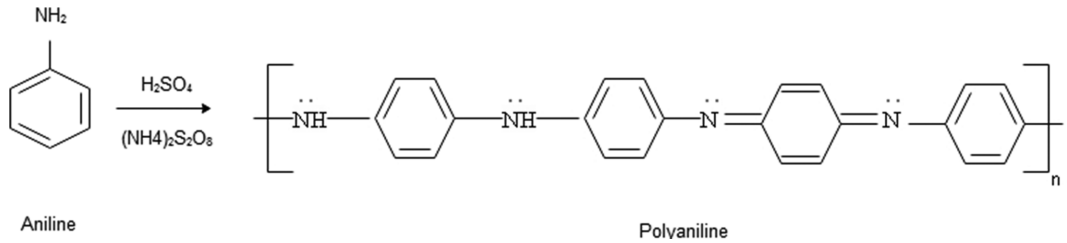


Fig. S1. The schematic of polyaniline polymerization process.

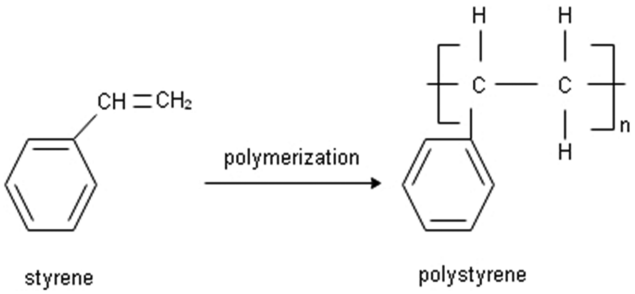


Fig. S2. The schematic of polystyrene polymerization process.

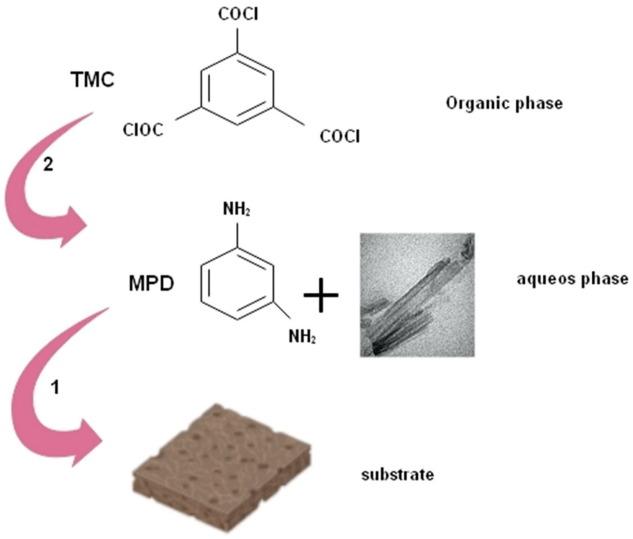


Fig. S3. The schematic of thin film membrane preparation.

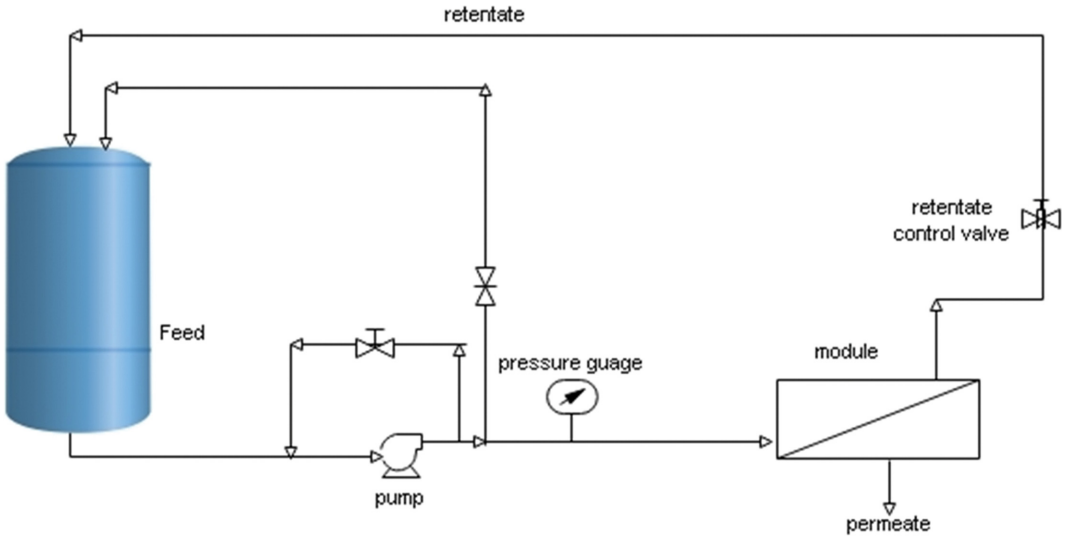


Fig. S4. Cross-flow NF setup for performance assessment of the membranes.

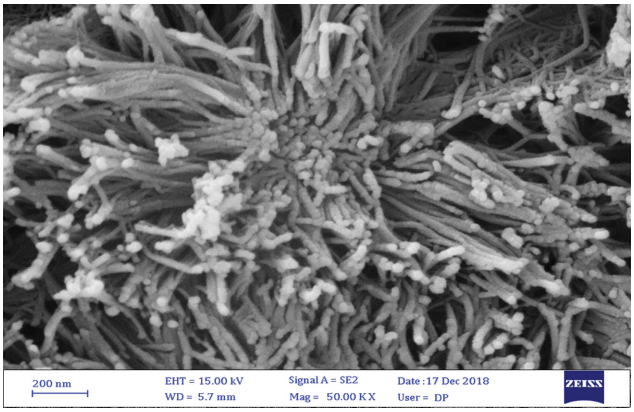


Fig. S5. FESEM image of the unmodified nanotube (TNT12).

Table S1. The results of AFM analysis for the neat TFC and TNT12 membranes

Membrane	RMS (nm)	R_a (nm)
TFC membrane	91.22	62.58
TNT12	63.34	46.91

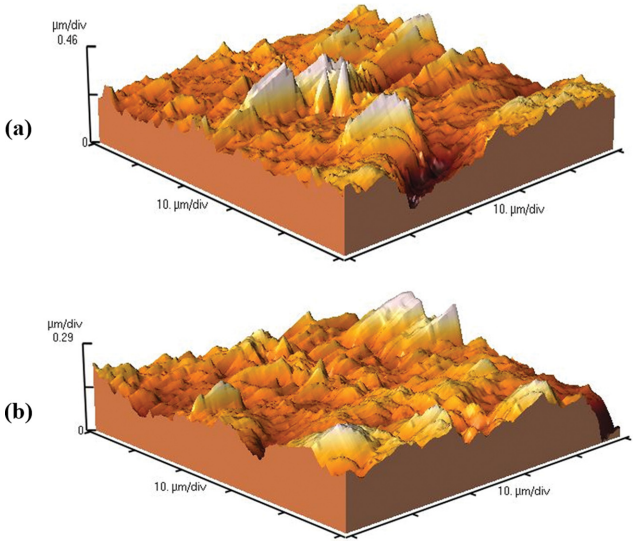


Fig. S6. 3D AFM images of (a) TFC and (b) TNT12 membranes.